Paper 4

Stéphane Teletchéa, **Tormod Skauge**, Einar Sletten and Jiří Kozelka.

" Cisplatin Adducts on a GGG Sequence Within a DNA Double-stranded Decamer Studied by NMR Spectroscopy and Molecular Dynamics Simulations"

(Manuscript to be submitted)

Cisplatin Adducts on a GGG Sequence Within a DNA Double-stranded Decamer Studied by NMR Spectroscopy and Molecular Dynamics Simulations

Stéphane Teletchéa,[a] Tormod Skauge,[b] Einar Sletten,[b] Jiří Kozelka*[a]

Abstract: The decanucleotide duplex [d($G_1C_2C_3G^*_4G^*_5G_6T_7C_8G_9C_{10}$)· d($G_{11}C_{12}G_{13}A_{14}C_{15}C_{16}C_{17}G_{18}G_{19}C_{20}$)] (G*G*G) intra-strand cross-linked at the G* guanines with the anti-tumour drug cisplatin (*cis*-[$PtCl_2(NH_3)_2$]) was studied by NMR and molecular dynamics (MD) simulations, in order to examine the structural perturbation of the duplex caused by intra strand GG platination within a GGG sequence. GGG sites have been shown to be hot spots of platination [1]. The NMR features of G*G*G were found to be similar to those of DNA duplexes cross-linked by cisplatin at a pyG*G*X site (X = C, T, A), indicating that a guanine 3′ to the G*G*-Pt cross-link does not particularly affect the structure. An unprecedented isomerization reaction on intact duplex state between 1,2 and 2,3 platination leads to a 40:60 equilibrium between G*G*G and GG*G* species. No tendency to inter strand cross-linking was observed. The deoxyribose of the 5′-G* adopts an N-type conformation while partial repuckering of the cytidines C3, C15 and C16 towards smaller average phase angles were found. The presence of a guanine 5′ to the G*G* cross-link induces structural perturbations significantly different from pyG*G* sequences. These conclusions were based on the combined analysis of 2D DQF-COSY, TOCSY, NOESY spectra and MD simulations.

Keywords: antitumor agents; molecular modelling; nuclear magnetic resonance; oligonucleotides; platinum

Abbreviations: TSP – Trisilylmethylphosphate, TMP – Trimethylphosphate, TEAA – Triethylacetic acid, G* - platinated guanine

---

[a] Dr. S. Teletchéa,[+] Dr. J. Kozelka
Laboratoire de Chimie et Biochimie Pharmacologiques et Toxicologiques
Université René Descartes, UMR 8601 CNRS
45, rue des Saints-Pères, 75270 Paris (France)
Fax: +331 42 86 83 87
E-mail: jiri.kozelka@univ-paris5.fr

[b] T. Skauge,[+] Prof. E. Sletten,
Department of Chemistry
University of Bergen
Allégt. 41
5007 Bergen (Norway)

[+] These two authors contributed equally to the present work.

Introduction

The antitumor activity of cisplatin (*cis*-[$PtCl_2(NH_3)_2$]) has motivated a number of structural studies on adducts that this compound forms with DNA, its likely principal cellular target. The most abundant adduct, the GG intra-strand cross-link, has received particular attention, and several groups investigated the structure of GG cross-linked double-stranded oligonucleotides. These all had the sequence pyG*G*X, where py = pyrimidine and X = T, C, or A (reviewed by Ano et al.[2] and by Riojas and Kozelka[3]). Interestingly G_n sequences (n≥3) are found to be hotspots of platination [1], but only two cisplatinated oligonucleotides containing d(GGG) sequences have been reported.[4, 5] In both cases, the GGG sequence reacted with cisplatin or its diaqua form to yield a mixture of the 1,2-GG and 2,3-GG cross-links. For the duplex, $d(AAGGGTACCCAT)_2$, G*4G*5 adducts gave a very stable hairpin form, while G*3G*4 adducts gave an ss-DNA coiled form.[4, 5] The ability of this special palindromic duplex ($T_m \approx 12°$ C) to form self-complementary hairpin forms, discouraged a detailed comparison with the results presented here as this study yielded only duplex DNA forms. An oligonucleotide platinated at a GGG site and subsequently annealed with its complementary strand to yield a stable duplex, has never before been studied by NMR.

We have recently improved the HPLC protocols for the separation of platinated oligonucleotides,[6] and decided to use this method to purify specific GGG cisplatin adducts (see Supplementary Information). The non-palindromic duplex [$d(G_1C_2C_3G^*_4G^*_5G_6T_7C_8G_9C_{10})\cdot d(G_{11}C_{12}G_{13}A_{14}C_{15}C_{16}C_{17}G_{18}G_{19}C_{20})$] (G*G*G), which is almost identical to the duplex [$d(G_1C_2C_3G^*_4G^*_5A_6T_7C_8G_9C_{10})\cdot d(G_{11}C_{12}G_{13}A_{14}T_{15}C_{16}C_{17}G_{18}G_{19}C_{20})$] (G*G*A) (GC pair exchange by a AT pair) studied previously,[7, 8] was chosen. This enabled us to compare the influence of the G4-G5 cisplatin adducts, G*G*G and G*G*A, on the duplex conformation. The substitution of 3′-G by 3′-A was previously predicted to stabilize a BII conformation at the A6pT7 step.[8] The platination was carried out on the top strand, using ^{15}N-labeled *cis*-[$PtCl_2(NH_3)_2$]. The two main adducts were separated by HPLC, and the major adduct, bearing the G4-G5 cross-link, was annealed with the complementary strand. The duplex was then studied by NMR & molecular dynamics simulations. We report here an unprecedented rearrangement of the G4-G5 adduct to G5-G6.

Results

NMR analysis of GGG and **G*G*G.**

Combined use of 2D NOESY, DQF-COSY and TOCSY spectra in D_2O[9-11] allowed the identification of all the non-exchangeable protons**,** except H5′/H5′′, of the unplatinated oligonucleotide duplex GGG and nearly all those of the G4-G5 platinated adduct G*G*G (Table 1). Exchangeable imino protons were assigned from NOESY spectra recorded in 90/10 H_2O/D_2O at 8°C.

A complete sequential walk could be carried out for G*G*G both in the H1′(n)-H6/8(n+1) and the H2′/H2′′(n)-H6/8(n+1) regions. Very weak C3H1′-G*4H8 and G*4H1′-G*5H8 NOE cross-peaks were observed (see Figure 1). This was also found for G*G*A and is a typical feature of pyG*G*-platinated DNA duplexes, caused by destacking between the platinated G* bases and between the 5′-G* and the preceding pyrimidine.[7] Destacking and tilting between the G* bases in the head-to-head fashion is further manifested in a relatively strong H8-H8 NOE. A very weak

G*4H1′-G*5H8 NOE is also indicative of destacking. All the B-DNA connectivities were found in the H2′/H2′′-H6/H8 region, in spite of the aforementioned destacking, which is in agreement with previous results for G*G*A. Further similarities between 2D NOESY spectra of G*G*G and other pyG*G* duplexes include weak H1′(n)-H8(n+1) and H3′(n)-H8(n+1) cross-peaks between the cytidine complementary to the 5′-G* (C17) and the following purine (G18), and a missing H3′(n)-H8(n+1) cross-peak at the py-G* (C3-G*4) step. We did observe the C16H1′-C17H6 cross-peak between the two cytidines complementary to G*pG* at medium intensity, whereas in previous reports, this peak is sometimes medium,[12, 13] and sometimes weak or missing.[7] This may be related to a variability of the sugar puckers reported for these cytidines (reviewed by Ano et al.[2], p. 272). The H1′(n)-H8(n+1) distance is fairly sensitive to the sugar pucker of nucleotide n, being longer for an N-pucker.[14] It is possible that C16 has more N character in G*G*A[7] than in G*G*G (vide infra).

At low temperature (281 K) imino-imino cross-peaks T7H3-G6H1 and T7H3-G13H1 are observed, while cross-peak G4H1-G5H1 is missing and G5H1-G6H1 is very weak.

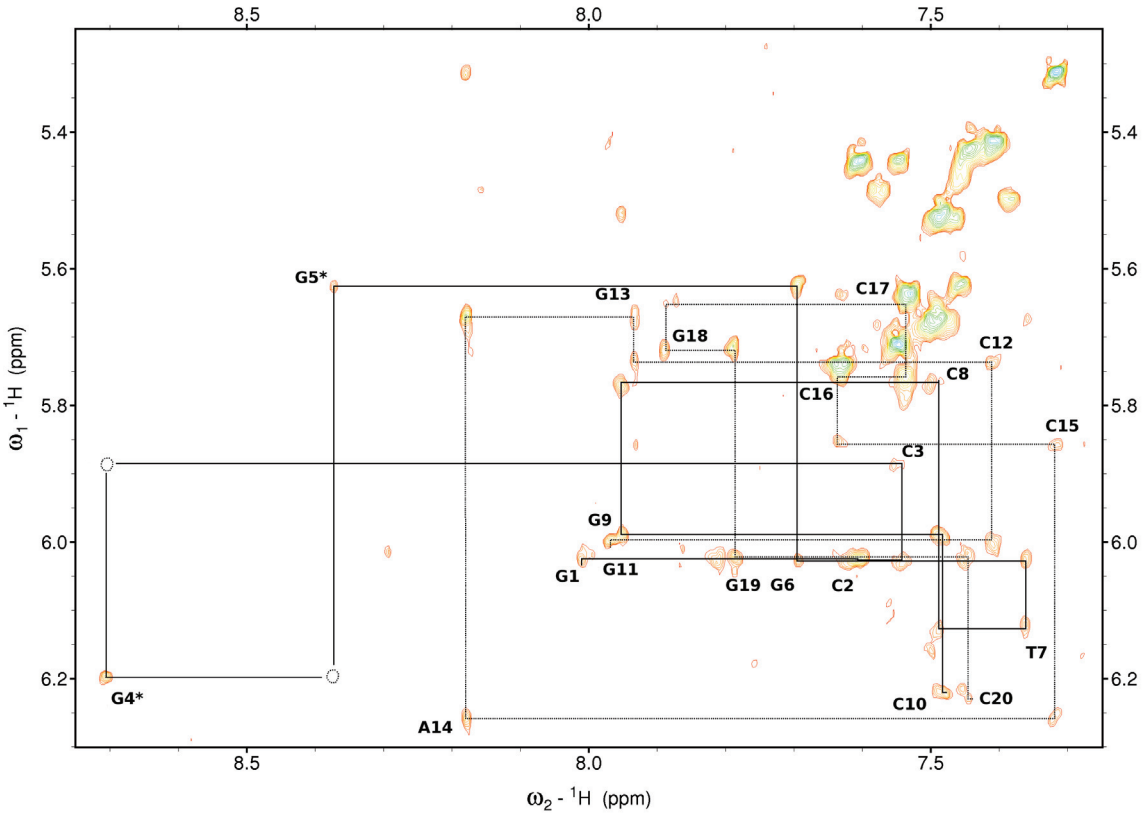

Figure 1: Expanded regions of NOESY spectra of d[($G_1C_2C_3G^*_4G^*_5G_6T_7C_8G_9C_{10}$)·d($G_{11}C_{12}G_{13}A_{14}C_{15}C_{16}C_{17}G_{18}G_{19}C_{20}$)] (G*G*G). The region shows the sequential walk for the platinated strand (a) and the complementary unplatinated strand (b) in the anomeric- aromatic region. Closed dotted circles indicate very weak peaks. Peaks not part

of the walk belong to the GG*G* duplex. Duplex concentration 0.50 mM in 55 mM phosphate buffer , 180 mM $NaClO_4$, pH 6.05 in D_2O at 305K.

Table 1. ^{1}H and ^{31}P chemical shifts of the duplexes GGG, G*G*G, and GG*G*. All spectra recorded at 305 K, except for the exchangeable protons for G*G*G and GG*G* recorded at 281 K. Shifts referenced to TSP and TMP for ^{1}H and ^{31}P, respectively. [a]Difference in chemical shift to that of pure GGG, [b]chemical shift value for this duplex oligomer.

	H8/H6	H2/H5/ CH3	H1´	H2´	H2´´	H3´	H4´	H1/H3	H41	H42	^{31}P
G1$_{GGG}$	7.98		6.01	2.65	2.78	4.85	4.26	n.a.			*n.a.*
G1$_{G*G*G}$[a]	*0.03*		*0.01*	*0.09*	*0.01*	*0.00*	*n.a.*	*(13.00)*[b]			*n.a.*
G1$_{GG*G*}$[a]	*0.02*		*0.01*	*0.05*	*0.01*	*n.a.*	*n.a.*	*n.a.*			*n.a.*
C2 $_{GGG}$	7.53	5.42	6.09	2.18	2.49	4.88	4.27		8.34	6.45	*n.a.*
C2 $_{G*G*G}$[a]	*0.08*	*0.03*	*-0.06*	*0.12*	*0.01*	*-0.04*	*-0.01*		*-0.05*	*0.02*	*n.a.*
C2 $_{GG*G*}$[a]	*0.02*	*0.02*	*0.01*	*0.02*	*0.01*	*0.01*	*n.a.*		*-0.10*	*-0.03*	*n.a.*
C3 $_{GGG}$	7.42	5.60	5.62	1.99	2.35	4.84	4.11		8.62	6.75	*n.a.*
C3 $_{G*G*G}$[a]	*0.13*	*0.11*	*0.27*	*-0.47*	*0.11*	*-0.13*	*-0.01*		*0.11*	*0.35*	*(-4.69)*[b]
C3 $_{GG*G*}$[a]	*0.04*	*0.02*	*-0.04*	*0.03*	*-0.03*	*0.00*	*n.a.*		*-0.09*	*0.09*	*n.a.*
G4 $_{GGG}$	7.83		5.64	2.66	2.76	4.99	4.34	13.07			*n.a.*
G*4 $_{G*G*G}$[a]	*0.88*		*0.56*	*-0.33*	*-0.01*	*0.18*	*-0.09*	*-0.02*			*(-3.12)*[b]
G4 $_{GG*G*}$[a]	*0.03*		*0.39*	*-0.10*	*0.00*	*-0.03*	*n.a.*	*-0.01*			*(-3.99)*[b]
G5 $_{GGG}$	7.67		5.81	2.64	2.74	4.96	4.39	12.95			*n.a.*
G*5 $_{G*G*G}$[a]	*0.70*		*-0.18*	*-0.23*	*-0.08*	*-0.13*	*-0.14*	*0.25*			*n.a.*
G*5 $_{GG*G*}$[a]	*0.62*		*0.21*	*-0.45*	*0.01*	*-0.18*	*n.a.*	*0.11*			*(-3.40)*[b]
G6 $_{GGG}$	7.53		5.92	2.47	2.73	4.83	4.37	12.82			*n.a.*
G6 $_{G*G*G}$[a]	*0.17*		*0.11*	*0.07*	*0.05*	*0.05*	*0.01*	*0.00*			*n.a.*
G*6 $_{GG*G*}$[a]	*0.42*		*-0.28*	*-0.23*	*-0.16*	*n.a.*	*n.a.*	*0.24*			*n.a.*
T7 $_{GGG}$	7.28	1.26	6.05	2.12	2.52	4.86	4.24	13.65			*n.a.*
T7 $_{G*G*G}$[a]	*0.08*	*0.04*	*0.08*	*0.09*	*0.04*	*0.06*	*0.04*	*0.08*			*n.a.*
T7 $_{GG*G*}$[a]	*0.22*	*0.06*	*0.12*	*0.13*	*0.04*	*0.05*	*0.03*	*0.20*			*n.a.*
C8 $_{GGG}$	7.47	5.64	5.73	2.04	2.41	4.85	4.13		8.53	6.83	*n.a.*
C8 $_{G*G*G}$[a]	*0.02*	*0.03*	*0.04*	*0.03*	*0.02*	*0.02*	*0.02*		*-0.11*	*0.03*	*n.a.*
C8 $_{GG*G*}$[a]	*0.03*	*0.04*	*0.04*	*n.a.*	*n.a.*	*n.a.*	*n.a.*		*-0.08*	*0.07*	*n.a.*
G9 $_{GGG}$	7.93		5.97	2.63	2.74	4.99	4.37	13.08			*n.a.*
G9 $_{G*G*G}$[a]	*0.02*		*0.02*	*0.03*	*0.02*	*0.02*	*0.03*	*-0.10*			*n.a.*
G9 $_{GG*G*}$[a]	*n.a.*		*n.a.*	*n.a.*	*n.a.*	*n.a.*	*n.a.*	*-0.10*			*n.a.*
C10 $_{GGG}$	7.46	5.48	6.20	2.19	2.18	4.50	4.06		n.a.	n.a.	*n.a.*
C10 $_{G*G*G}$[a]	*0.03*	*0.04*	*0.03*	*0.00*	*0.03*	*0.03*	*0.02*		*(8.16)*[b]	*(6.63)*[b]	*n.a.*
C10 $_{GG*G*}$[a]	*n.a.*	*n.a.*	*n.a.*	*n.a.*	*n.a.*	*n.a.*	*n.a.*		*n.a.*	*n.a.*	*n.a.*

	H8/H6	H2/H5/ CH3	H1´	H2´	H2´´	H3´	H4´	H1/H3	H41	H42	^{31}P
G11 $_{GGG}$	7.96		5.99	2.60	2.78	4.85	4.24	n.a.			*n.a.*
G11 $_{G*G*G}$[a]	*0.01*		*0.01*	*0.00*	*0.02*	*0.02*	*n.a.*	*(12.99)* [b]			*n.a.*
G11 $_{GG*G*}$[a]	*n.a.*		*n.a.*	*-0.32*	*n.a.*	*n.a.*	*n.a.*	*n.a.*			*n.a.*
C12 $_{GGG}$	7.39	5.40	5.71	2.02	2.39	4.87	4.17		8.49	6.48	*n.a.*
C12 $_{G*G*G}$[a]	*0.02*	*0.02*	*0.03*	*0.04*	*0.04*	*0.02*	*0.03*	*0.00*	*-0.11*	*n.a.*	*n.a.*
C12 $_{GG*G*}$[a]	*0.03*	*0.02*	*0.06*	*n.a.*	*n.a.*	*n.a.*	*n.a.*	*0.00*	*-0.10*	*-0.01*	*n.a.*
G13 $_{GGG}$	7.91		5.61	2.72	2.81	5.03	4.36	12.87			*n.a.*
G13 $_{G*G*G}$[a]	*0.02*		*0.06*	*0.05*	*0.03*	*0.03*	*n.a.*	*-0.07*			*(-3.92)*[b]
G13 $_{GG*G*}$[a]	*0.03*		*0.11*	*n.a.*	*n.a.*	*n.a.*	*n.a.*	*-0.05*			*n.a.*
A14 $_{GGG}$	8.16	7.87	6.25	2.70	2.91	5.03	4.48				*n.a.*
A14 $_{G*G*G}$[a]	*0.02*	*0.06*	*0.01*	*0.07*	*-0.02*	*0.00*	*0.01*				*(-4.02)*[b]
A14 $_{GG*G*}$[a]	*0.02*	*0.03*	*0.04*	*-0.02*	*-0.05*	*n.a.*	*n.a.*				*(-4.06)*[b]
C15 $_{GGG}$	7.23	5.24	5.79	2.03	2.42	4.74	4.18		8.02	6.48	*n.a.*
C15 $_{G*G*G}$[a]	*0.09*	*0.08*	*0.07*	*0.05*	*0.06*	*0.01*	*-0.02*		*0.17*	*0.26*	*n.a.*
C15 $_{GG*G*}$[a]	*0.23*	*0.29*	*0.16*	*-0.03*	*-0.03*	*0.05*	*n.a.*		*0.28*	*0.34*	*n.a.*
C16 $_{GGG}$	7.44	5.44	5.90	2.08	2.42	4.80	4.14		8.34	6.55	*n.a.*
C16 $_{G*G*G}$[a]	*0.19*	*0.30*	*-0.14*	*-0.02*	*0.06*	*0.02*	*0.01*		*0.17*	*0.48*	*n.a.*
C16 $_{GG*G*}$[a]	*0.13*	*0.05*	*0.08*	*0.03*	*0.03*	*0.00*	*n.a.*		*-0.25*	*0.13*	*n.a.*
C17 $_{GGG}$	7.40	5.57	5.57	1.98	2.34	4.82	4.09		8.59	6.74	*n.a.*
C17 $_{G*G*G}$[a]	*0.13*	*0.07*	*0.08*	*0.00*	*-0.03*	*0.00*	*-0.02*		*-0.49*	*-0.01*	*n.a.*
C17 $_{GG*G*}$[a]	*-0.01*	*-0.07*	*0.06*	*0.02*	*0.02*	*0.02*	*n.a.*		*-0.28*	*0.08*	*n.a.*
G18 $_{GGG}$	7.85		5.65	2.68	2.76	4.99	4.34	13.16			*n.a.*
G18 $_{G*G*G}$[a]	*0.04*		*0.07*	*0.04*	*0.03*	*0.01*	*0.07*	*-0.27*			*n.a.*
G18 $_{GG*G*}$[a]	*0.02*		*-0.01*	*0.02*	*n.a.*	*0.01*	*n.a.*	*-0.09*			*n.a.*
G19 $_{GGG}$	7.76		5.99	2.54	2.74	4.97	4.38	13.12			*n.a.*
G19 $_{G*G*G}$[a]	*0.03*		*0.04*	*0.05*	*0.04*	*0.03*	*n.a.*	*-0.07*			*n.a.*
G19 $_{GG*G*}$[a]	*0.05*		*0.04*	*0.05*	*0.03*	*0.03*	*n.a.*	*-0.06*			*n.a.*
C20 $_{GGG}$	7.43	5.42	6.18	2.17	2.19	4.50	4.04		n.a.	n.a.	*n.a.*
C20 $_{G*G*G}$[a]	*0.02*	*0.01*	*0.04*	*0.04*	*0.03*	*0.03*	*0.04*		*(8.14)*[b]	*(6.56)* [b]	*n.a.*
C20 $_{GG*G*}$[a]	*0.03*	*0.05*	*0.04*	*n.a.*	*n.a.*	*n.a.*	*n.a.*		*n.a.*	*n.a.*	*n.a.*

Table 1 indicates that the chemical shifts of G*G*G show all the typical features of platinated pyG*G* duplexes [2]. In particular, the two downfield-shifted H8 resonances of G*4 and G*5 confirm that these bases are platinated, and the chemical shifts are characteristic of all pyG*G* adducts characterized thus far (i.e. ~8.7 ppm for the 5´-G* and 8.0-8.4 ppm for the 3´-G*). The

resonance of the pyH2′ on the 5′-side of G* is always found to be strongly upfield shifted (~1.5 ppm). Additionally, this shift is found to be correlated with the H2′ of the cytidine complementary to 5′-G* for most of the pyG*G* adducts[8]. In G*G*G, the C3-H2′and C17-H2′ shifts are 1.52 and 1.98 ppm, respectively, (Table 1, compare with Figure 13 of Elizondo-Riojas et al.[8]), i.e. reasonably close to the correlation line. All these spectral features suggest that the structure of G*G*G is similar to that of pyG*G*X (X = A, C, T).[7, 12, 13, 15-17]

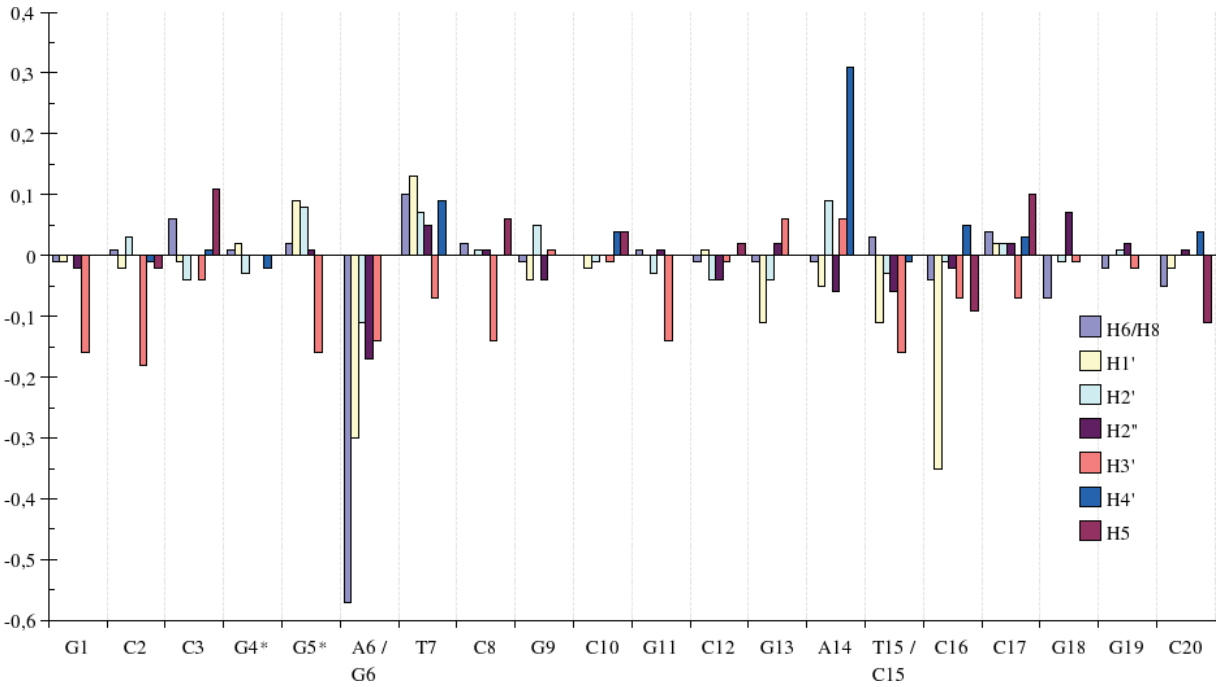

Figure 2: Differential chemical shifts of the non-exchangeable protons of G*G*G minus G*G*A. From spectra recorded at 305K (G*G*G) and 298K (G*G*A).

Comparison between the chemical shifts of the non-exchangeable protons of G*G*G and G*G*A (Figure 2) suggests that large parts of these duplexes must be virtually superimposable. Significant differences include the shifts of G6/A6, which is plausible, since guanosine and adenosine sugar protons have intrinsically different shifts,[18] and those of C16, which is plausible as well, since the 5′-base is mutated from T to C, which has a stronger ring current effect.[19] The structural similarity between G*G*G and G*G*A is further supported by similar features seen in the ^{31}P NMR spectra (vide infra).

Analysis of sugar puckers: Cisplatin coordination is known to alter the sugar puckers of nucleotides at the platination site. In all the reported pyG*G* cases, the 5′-G* repuckers from the normal S form to virtually 100% N. The cytidine nucleotides complementary to the G*G* cross-link have been reported as N/S, S/S and S/N for the cytidines C/C complementary to the 3′-G* and 5′-G*, respectively.[2] We have analysed the NMR data with particular attention paid to the sugar pucker of the central CG*G*•CCG trinucleotide.

Information from $J_{1'2'}$ and $J_{1'2''}$ coupling constants: DQF-COSY spectra recorded on a 600 MHz spectrometer using a cryoprobe enabled us to extract most of the $J_{1'2'}$ and $J_{1'2''}$ couplings with an

estimated precision of ±0.6-1.0 Hz (Table 2). Most of the nucleotides show $J_{1'2'}$ values close to 10 Hz and $J_{1'2''}$ values close to 5 Hz, characteristic of S sugar puckers in B-DNA.[20] Four nucleotides have sugar puckers that deviate from the S conformation: C3, G*4, C15 and C16. As expected, G*4 shows a small $J_{1'2'}$ of 1.9 Hz and a large $J_{1'2''}$ of 7.1 Hz, values compatible with a 100% N pucker.[20] Both the cytidines complementary to the G*G* cross-link show intermediate values. For C3, the observed $J_{1'2'}$ and $J_{1'2''}$ coupling constants of 4.5 and 8.0 Hz, respectively, are similar to those observed previously by Herman et al. for G*G*A ($J_{1'2'}$ = 4.5; $J_{1'2''}$ = 6.5 Hz)[7] The slightly larger $J_{1'2''}$ coupling constant observed for G*G*G indicates that the conformational equilibrium is shifted more towards N than in G*G*A. The MD simulation of solvated G*G*G (vide supra) indicated a major N conformation with a phase angle P of ~25º and an amplitude ϕ_m of ~38º, for which the $J_{1'2'}$ and $J_{1'2''}$ values are, according to Rinkel and Altona,[20] 2.4 and 8.6 Hz, respectively. If we assume that the actually observed values result from an admixture of a minor percentage of the classical S conformation (P=156º, ϕ_m=35º, $J_{1'2'}$ =10.2, $J_{1'2''}$ =5.7 Hz), then an optimisation shows that 75% N and 25% S yield the coupling constants of $J_{1'2'}$ = 4.3 and $J_{1'2''}$ =7.9 Hz, in good agreement with the observed values. For G*G*A, 60-70% N was estimated for C3; thus the difference between the two sugar conformations is not large.

Information from NOESY data: Intranucleotide H2´-H6/8 and H3´-H6/8 distances depend on the phase angle P and are also dependent on the glycosidic angle χ,[9]. Since there was no indication of any *syn* sugars in G*G*G, the distances can be considered to depend solely on the phase angle P and therefore be utilized to give a qualitative estimate of the sugar conformation.[9, 20, 21] NOE distances derived from three different NOESY experiments (80 and 200 ms mixing time at 305K in D_2O, and 200 ms mixing time at 281K in 90% H_2O) were combined to determine the average apparent intranucleotide H2´-H6/8 ($d_{H2'app}$) and H3´-H6/8 ($d_{H3'app}$) distances, using the cytidine H5-H6 (2.45 Å) cross-peaks as reference (see Table 2). The ratio $d_{H2'app}/d_{H3'app}$ was then used as indicator for the percentage of S sugar conformation assuming a two-state N↔S equilibrium.

In a solution mixture containing the fraction x_S of S pucker and (1-x_S) of N pucker for a given nucleotide, the H2´-H6/8 NOE is proportional, in absence of spin diffusion, to $x_S*V_{H2'S}$ + (1-x_S)*$V_{H2'N}$, where $V_{H2'S}$ and $V_{H2'N}$ are the H2´-H6/8 NOE volumes in the S and N conformations, respectively. The apparent H2´-H6/8 distance $d_{H2'app}$ determined from this NOE volume is then proportional to $[x_S*d_{H2'S}^{-6} + (1-x_S)*d_{H2'N}^{-6}]^{-1/6}$, where $d_{H2'S}$ and $d_{H2'N}$ are the H2´-H6/8 distances in the S and N conformations. Similarly, the apparent $d_{H3'app}$ distance is proportional to $[x_S*d_{H3'S}^{-6} + (1-x_S)*d_{H3'N}^{-6}]^{-1/6}$, with $d_{H3'S}$ and $d_{H3'N}$ being the H3´-H6/8 distances in the S and N conformations, respectively. The ratio $d_{H2'app}/d_{H3'app}$ is then defined as in Eq. (1).

$$\frac{d_{H2'app}}{d_{H3'app}} = \left[\frac{x_S \cdot d_{H2'S}^{-6} + (1-x_S) \cdot d_{H2'N}^{-6}}{x_S \cdot d_{H3'S}^{-6} + (1-x_S) \cdot d_{H3'N}^{-6}} \right]^{-1/6} \qquad (1)$$

Average values of $d_{H2'S}$ and $d_{H2'N}$ were extracted from a large number of energy minimized MD models of B-DNA oligonucleotides, yielding 2.45±0.32 and 3.27±0.24 Å, respectively, and those of $d_{H3'S}$ and $d_{H3'N}$ yielding 4.49±0.26 and 2.27±0.26 Å, respectively. Using these averages and Eq. (1), the ratio $d_{H2'app}/d_{H3'app}$ as a function of x_S was plotted in Figure 3. Due to the large error limits for the experimental values the S-shaped function could be approximated by the linear

equation (Eq. 2) which was used to calculate the percentages of S for all the nucleotides of G*G*G, (Table 2).

$$\frac{d_{H2'app}}{d_{H3'app}} = x_S\left(\frac{d_{H2'S}}{d_{H3'S}} - \frac{d_{H2'N}}{d_{H3'N}}\right) + \frac{d_{H2'N}}{d_{H3'N}} \approx x_S\left(\frac{2.45}{4.49} - \frac{3.27}{2.27}\right) + \frac{3.27}{2.27} \qquad (2)$$

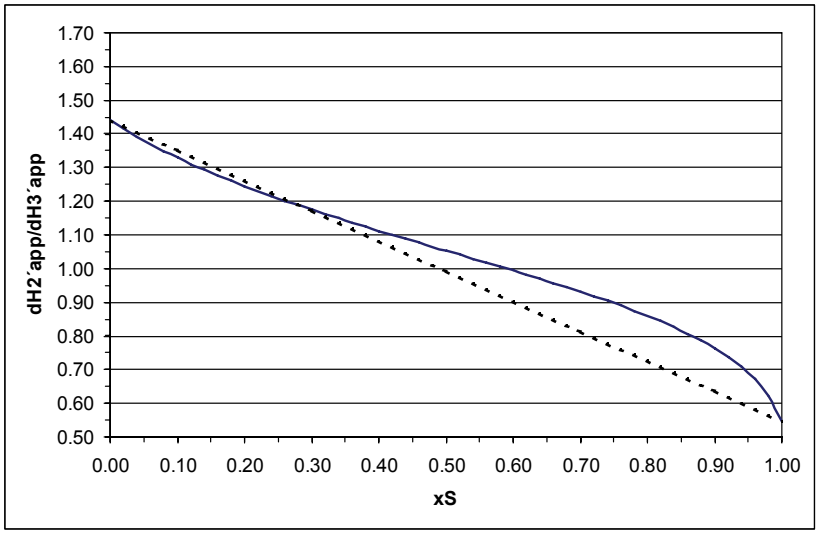

Figure 3. Plot of the ratio of apparent distances $d_{H2'app}/d_{H3'app}$ in a two-state N↔S equilibrium, as a function of the fraction of S conformation, x_S, according to Eq. (1). The dashed line represents the approximated linear equation

In Table 2, one can see that most of the nucleotides show a pucker ratio H2´-H6/8/H3´-H6/8 of 0.7 or less, corresponding to a predominantly S pucker. G*4, on the other hand, has a ratio of 1.465 typical for N pucker. Intermediate values are observed for C3, C15, and C16. N↔S equilibria were already indicated for C3 and C15 from DQF-COSY data, whereas C16 showed $J_{1'2'}$ and $J_{1'2''}$ couplings typical for S sugars. MD simulations for G*G*A showed that C16 undergoes frequent transitions between N and S conformations, and for G*G*G, the C16 N conformation is clearly preponderant (vide infra). The ensemble of these data suggests that C16, the cytidine complementary to the 3´-G*, shows an N↔S conformational equilibrium shifted towards N.

For C15, the MD simulation (vide infra) revealed transitions between "south" (P≈125º, ϕ_m≈40º), "north" (P≈25º, ϕ_m≈35º), and "east" (P≈75º, ϕ_m≈38º) type. These values correspond to the coupling constants: $J_{1'2'}$ ≈10.5, $J_{1'2''}$ ≈5.2 (S), $J_{1'2'}$ ≈7.1, $J_{1'2''}$ ≈8.2 (E), $J_{1'2'}$ ≈2.3, $J_{1'2''}$ ≈8.4 (N) .[20] An iterative optimisation of the individual fractions (73 % N, 14% E and 13 % S) yields $J_{1'2'}$ = 4.0 and $J_{1'2''}$ = 8.0 Hz, in good agreement with the experiment.

Table 2. Spin-spin couplings $J_{1'2'}$, $J_{1'2''}$ and $\Sigma 1'$ determined from DQF-COSY spectra, interproton distances H2′-H6/8 and H3′-H6/8 determined from NOESY spectra, and the ratio H2′-H6/8/H3′-H6/8, for the platinated duplex G*G*G. Not all values were possible to assign due to spectral overlap. [a] Percentage of S conformation calculated from J-coupling values,[20] [b] Percentage of S conformation calculated from the d(H2′-H6/8)/d(H3′-H6/8) distance ratio using Eq.(2) (see text).; [c] $\Sigma 1' = J_{1'2'} + J_{1'2''}$.

Base	$J_{1'2'}$	$J_{1'2''}$	$\Sigma 1'$ [c]	$\%S_J$ [a]	d(H2′-H6/8)	d(H3′-H6/8)	Ratio	$\%S_{NOE}$ [b]
G1					2.61	4.53	0.576	97
C2	8.0	5.2	13.0	81	2.44	3.83	0.637	90
C3	4.5	8.0	11.4	36	3.03	3.20	0.948	44
G*4	1.9	7.1	10.4	12	3.74	2.55	1.465	-3
G*5	8.8	4.4	13.5	89	2.90	4.09	0.709	82
G6					2.80	4.85	0.578	96
T7	9.5	4.9	14.5	90	2.46	3.84	0.640	89
C8	9.7	5.2	14.9	86	1.83	3.05	0.602	94
G9					1.99	3.59	0.553	99
C10					2.20	3.30	0.668	86
G11					2.39	4.01	0.595	94
C12	10.0	5.0	16.3	98	1.86	4.25	0.438	112
G13					2.22	4.50	0.492	106
A14	8.8	5.3	14.0	87	2.66	3.49	0.760	76
C15	4.0	7.7	12.4	45	2.90	3.34	0.868	64
C16	9.1	4.6	13.7	84	2.52	2.70	0.933	57
C17	11.0	4.4	15.8	96	2.45	4.80	0.510	104
G18					2.68	3.80	0.705	82
G19					2.73	4.28	0.638	90
C20						3.42		

The calculated fractions of S pucker from NOESY-derived distances are sometimes larger than 100% or lower than 0%, due to the uncertainty in the calculated distances. Estimated uncertainty in %S is ~ 25 %.

Search for BII substates using ^{31}P and ^{1}H NMR: The phosphate backbone conformations may be classified as either BI or BII. These conformations are characterized by coupled transitions in the torsion angles ε (C4′-C3′-O3′-P) and ζ (C3′-O3′-P-O5′). For BI the (ε,ζ) angles are (t,g^-), while they are (g^-,t) for BII.[22] Intra- and inter-strand stacking interactions have been suggested to be responsible for observed sequence-dependent shifts of the BI↔BII equilibrium.[23] Evidence for a mechanical coupling of phosphate BI↔BII transitions to deoxyribose N↔S transitions was put forward by Isaacs and Spielmann.[24] The BI-BII equilibria have been found to

play an important role in the protein recognition of DNA, e.g. in the NF-κB recognition of DNA.[25] Two-dimensional ^{1}H-^{31}P heteronuclear correlation NMR spectra (HETCOR) was used to assess the position of the BI↔BII equilibria.

MD simulations for G*G*A[8] have indicated that the A6pT7 step partly adopts a BII conformation stabilized by a hydrogen bond between an NH_3 ligand of platinum and the A6-N7 atom. For the G*G*G duplex, where the analogous hydrogen bond to G6-N7 is supposed to be stronger, the G6pT7 step may be preponderantly BII leading to a downfield ^{31}Pshift.[26] However, the ^{31}P spectrum of G*G*G shows only one significantly downfield shifted signal. The signal at about 1 ppm downfield from the main cluster of peaks was assigned to the G*4pG*5 phosphate. A similar ^{31}P downfield shift for was found for G*G*A[7] and is a common feature of pyG*G* platinated duplexes.[2] Both G*G*G and G*G*A show a ^{31}P upfield-shifted signal, assigned in both cases to the C3pG*4 phosphate. The present data therefore does not support the hypothesized BII-conformation stabilized by the cisplatin amino - 3´X-N7 hydrogen bond. The reason for the discrepancy could be due to an overestimation of this bond by the Amber/parm98 forcefield.

Reversible G*G*G ↔ GG*G* isomerization. While the NMR analysis was in progress for the duplex, it became evident that the sample contained not one but two platinated DNA duplex species. Nine days after annealing the platinated strand, one major (~70 %) and one minor (~30 %) species were observed. The major species was assigned as the G*G*G sequence, while the minor as the GG*G* sequence (*vide infra*). A slow transition from 70:30 (G*G*G:GG*G*) occurred reaching a final equilibrium of approximately 40:60 after 200-300 days. The kinetics of this interconversion is visualized in Figure 4 where the relative averaged peak volumes of the cytidine H5-H6 cross-peaks (the average of between 3 and 9 H5-H6 cross-peak volumes, depending on spectral overlap and resolution, was used for each species) taken as a measure of the percentages of both species are plotted as a function of effective time, t_{eff}. The need for an effective time variable came from the fact that the sample was exposed to several temperatures during the long period the sample was studied. It was assumed that negligible rearrangement took place below 4 deg C. The time period t_{eff} was therefore calculated as $t_{eff} = 2t(T-277)/10$, where t is the real time period which the sample spent at the actual temperature. This corresponds to doubling the interconversion rate when the temperature is increased by 10 K.[27] The rate constants for the isomerization reaction can then be calculated assuming a reversible first order reaction.

For a reversible conversion of species A to species B, the differential equations are

$$\frac{dA}{dt} = -k_f \cdot A + k_b \cdot B \qquad (3)$$

(k_f and k_b are the forward and backward rate constants)
If at t=0, the A concentration is A_0 and that of B is zero, we obtain for A as a function of time:

$$A = A_0 \frac{1}{(k_f + k_b)}\left[k_b + k_f e^{(-k_f + k_b)t}\right] \qquad (4)$$

The experimental points of Figure 4 were fitted to Eq.(4). The fit shown in Figure 4 is fairly good, suggesting that our hypothesis of a reversible rearrangement of G*G*G to GG*G* in solution is realistic.

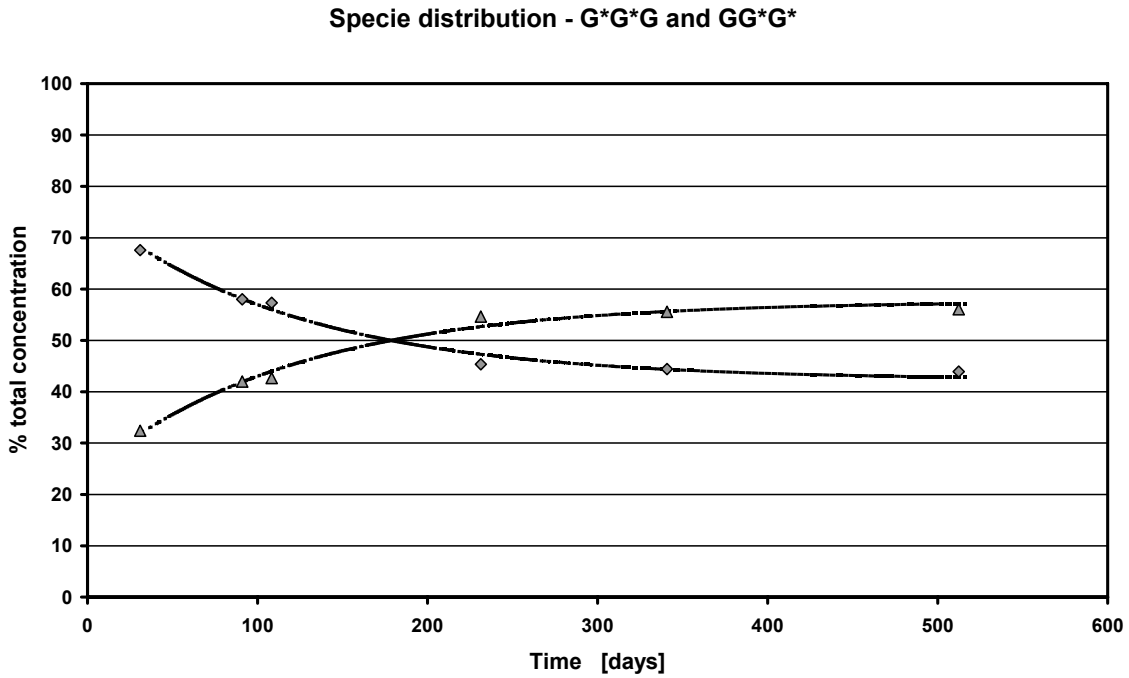

Figure 4. Kinetics of the rearrangement of G*G*G to GG*G*. Lines are the exponential fit of Eq. (4) to the experimentally determined concentration ratios. Time calculated as effective time (see text). The time of annealing the platinated strand with it's complementary strand is set as $t_{eff} = 0$.

It is currently unclear whether the ~30 % amount of GG*G* present at the time of the recording of the first 2D NMR spectrum (~25 % at $t_{eff} = 0$) originated from an incomplete HPLC separation or whether interconversion took place during the subsequent manipulation of the platinated single strand and its hybridisation with the complementary strand (see Experimental Section and Supplementary Information).

Analysis of the NOESY spectra of the equilibrated sample using a 600 MHz spectrometer equipped with a cryoprobe identified the second species as the cross-linked duplex, GG*G*. This was apparent from i) the complete H1′(n)-H6/8(n+1) and H2′/2′′(n)-H6/8(n+1) sequential walk that could be followed for GG*G* (except for terminal residues due to complete signal overlap with G*G*G), ii) the relatively strong G5H8-G6H8 cross-peak characteristic of a GpG intra-strand adduct (Figure 5), iii) the observation of a downfield shifted ^{31}P signal for G*5pG*6. The ^{31}P signal was assigned from ^{1}H-^{31}P HETCOR by it's connectivity to H3′ and H4′. Table 1 gives the chemical shifts of GG*G*.

An inspection of the chemical shifts for GG*G* (Table 1) shows that the G*5-H8 signal is significantly less downfield shifted (0.62 ppm) than what is usually found in pyG*G* containing duplexes.[7, 15, 28] The chemical shift of G*-H8 on the 5′-side was reported to have downfield shifts in the range ~0.9 ppm and to be insensitive to the 5′ flanking base (C or T). The downfield shift observed for the G*-H8 on the 3′- side (0.42 ppm) is within the normal range (~0.5 ppm). Most significant is the unusually small upfield shift (0.10 ppm) observed for the G-H2′ signal of the nucleotide on the 5′-side to the cross-link. This H2′ signal is found to be upfield shifted ca 0.8 ppm in all platinated cross-linked duplexes studied so far. It has been suggested that this characteristic H2′ shift originates from the ring current of the 5′-G* into whose shielding cone the H2′ proton

penetrates.[8] Other typical NMR spectral features of general pyG*G* cross-links *not* seen in GG*G* : i) the H1′ resonance of the nucleotide 5′ to the G*G* cross-link is 0.1-0.2 ppm upfield-shifted; ii) the H3′ resonance of the 5′-G* is ~0.2 ppm downfield-shifted and iii) the H2′ resonance of the cytidine complementary to the 5′-G* is slightly upfield-shifted. However, it should be noted for iii) that the 3′ flanking base in this sequence is a cytosine, while in all other sequences it is a guanine. The lack of these typical spectral features indicate that the 5′- GG* step in GG*G*- is significantly different from that of the 5′-pyG*. This conclusion is further corroborated by the observation of strong H2′-H8 and moderate H3′-H8 cross-peaks of G4, suggesting an S conformation for the sugar, whereas in the pyG*G* duplex adducts, this nucleotide has partly or entirely N pucker.

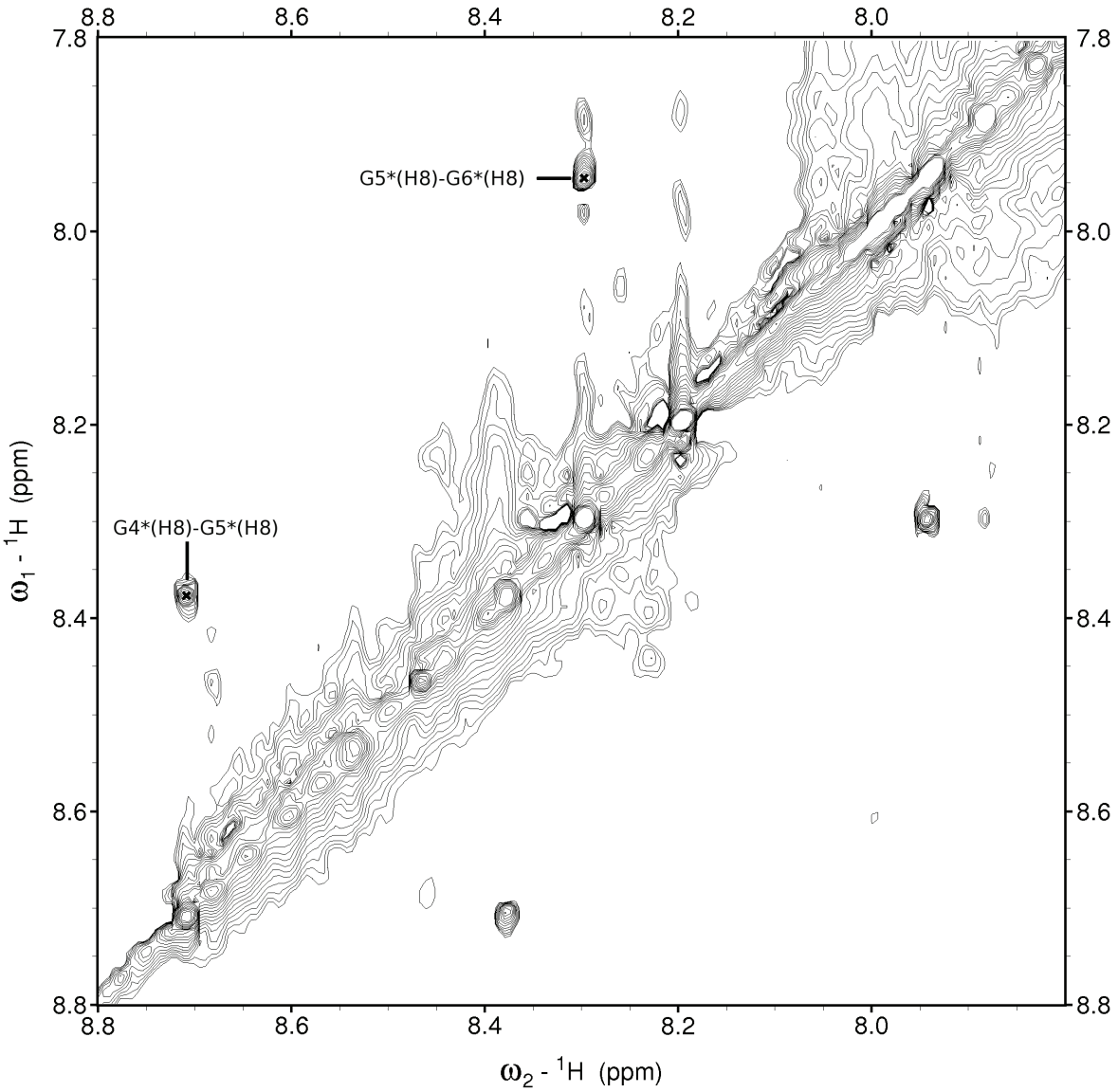

Figure 5. Expanded region of a NOESY spectrum of the mixture G*G*G/GG*G*. The region shows the H8-H8 cross-peaks between the platinated G*G* for G*G*G and GG*G*, respectively. Total duplex concentration (major and minor species) 0.50 mM in 55 mM phosphate buffer , 180 mM $NaClO_4$, pH 6.05 in D_2O at 281 K.

Interestingly, similar spectral features have been found for the duplex [d(CCTCAG*G*CCTCC)· (GGAGGCCTGAGG)] cross-linked at G*pG* with $Pt(DACH)^{2+}$ (DACH = trans-1,2-diaminocyclohexane).[29] The differences were ascribed to the presence of the DACH ligand which is sterically more demanding than the two NH_3 groups of cisplatin. This argument was supported by molecular models of the AG*G*-Pt(DACH) adduct which showed a significantly smaller kink angle than the models proposed previously for the pyG*G*-$Pt(NH_3)_2$ adducts. From the resemblance between the NMR features of the AG*G*-Pt(DACH) containing duplex and those of our GG*G* adduct (Figure 6), we propose that the factor responsible for the differences between the pyG*G*-$Pt(NH_3)_2$ series on one hand, and the AG*G*-Pt(DACH) on the other hand, is the purine 5′ to the G*pG* cross-link, rather than the diamine ligand. We believe that the smaller kink angle found for the AG*G*-Pt(DACH) duplex may have originated from differences in the molecular modelling procedures. A detailed structural study of GG*G* will be reported elsewhere.

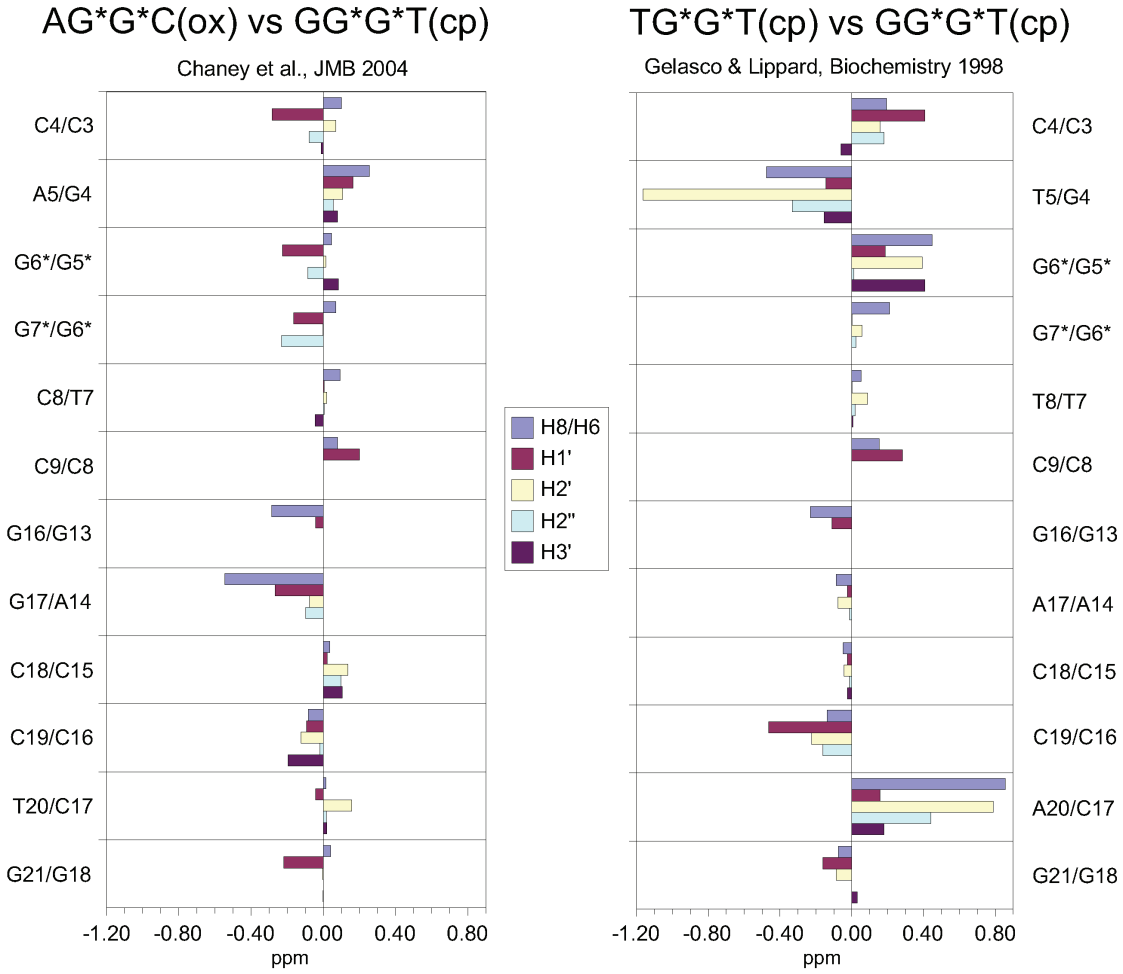

Figure 6. Chemical shift differences between the GG*G* sequence and (left) the AG*G*C(ox) NMR solution structure reported by the Chaney group[29] and (right) TG*G*T(cp) NMR solution structure reported by Gelasco & Lippard.[13] Experimental conditions for (left) AG*G*C(ox): 1.9 mM duplex concentration, 100 mM NaCl, pH 7.0, 5 mM Na_2HPO_4/NaH_2PO_4, 298 K, (right) TG*G*T(cp): 3.2 mM duplex concentration, 100 mM NaCl, pH 6.9, 10 mM Sodium Phosphate, 288K.

Molecular dynamics simulations of G*G*G with explicit solvent.
Molecular dynamics (MD) simulations of G*G*G were accomplished using Amber6 and the forcefield parm98 extended with improved parameters describing the platinum coordination.[3, 7] The simulations were run without restraints and subsequently compared with the experimental NMR data.[8] The first 10 ns of the 20 ns production period showed two reversible transitions of the preponderantly N pucker of G*4 to S. These transitions were an obvious artefact since the NMR data showed virtually 100% N pucker, in accordance with all available data on G*pG*-platinated DNA duplexes.[30-35] The parm98 forcefield was developed from parm94 and one of the major modifications was to shift the N↔S equilibrium of the sugar puckers more towards S conformations.[36] It is therefore possible that the cisplatin parameters developed for parm94, when used with parm98, results in a too high degree of S conformation on puckers belonging to platinated 5′-G*. As a result, only the last 10 ns of the production period, where the sugar pucker of the G*4 residue remained N throughout, was used for structural analysis.
The MD simulation was in good agreement with the 2D NOESY derived distances. A total of 221 NOE distances were extracted, of which 96 belonged to the interaction site as defined by the context d(-CG*G*G-)·(-CCCG-). Assuming an uncertainty of 0.60 Å of both the NMR and the MD, only 10 distances within the interaction site had deviations larger than the uncertainty (Table S3). Of those 10 distances, 5 could be explained by spin diffusion or crosspeak overlap (details in Supplementary Information). The structure of the G*G*G oligomer, averaged over 10 ns, is shown in Figure 7.

The helix is kinked 67±9° towards the major groove, localized at the platination site. The roll between G*4 and G*5 is 74±3°. Sugar puckers are all 96-100 % S, except C3 and G*4 having 22 and 21 % S, respectively, and C15 and C16 having 66 and 5 % S, respectively. The sugar puckers are in good agreement with the NMR data, except for C3, G*4 and C16 (see Supplementary Information).

In G*G*A, the MD simulations showed that BII was the major conformation for the A6-T7 step 3′ to G*4-G*5.[8] This was explained by the presence of a hydrogen bond between A6-N7 and the 3′ amino group of cisplatin. An exchange of an adenine for a guanine (which has a more basic N7 (ref)) is expected to result in a stronger hydrogen bond and a stabilizing effect on the BII conformation. However, our ^{31}P NMR data ruled out the possibility of a stable BII conformation for G*G*G and the MD show a stable BI throughout the simulation time. Nonetheless, the G6-N7 – cisplatin-NH_3 hydrogen bond is present 75 % of the simulation. A more thorough analysis revealed an α/γ equilibrium $g^+/g^- \leftrightarrow t/t$ for the G6pT7 phosphate and this transition is known to disfavour the BII conformation.[37] The unusual α/γ - *t/t* conformation induces an unwinding which could be responsible for the observed sugar pucker phases of C3 and C16.

The G*4-G*5 adduct shows a flexible py-G*4′ step. A salient observation of the previous MD simulation of G*G*A was a lateral movement between the C3/G18 and G*4/C17 base pairs, allowing the sugar residue of C3 to penetrate temporarily the shielding cone of G*4. Evidence for this result from molecular modelling came from the upfield shifts of the H2′ signals of C3 and C17.[8] The lateral movement was quantitatively manifest in the plots of the helicoidal parameter slide of the steps C3-G*4 and C17-G18 which attained values of ~1, characteristic of the C3 sugar entering the shielding cone of G*4 and the C17 sugar that of G18. Figure 8 shows the slide parameter of the step C3/G*4 as a function of simulation time. This figure can be compared with

Figure 1 of Elizondo-Riojas and Kozelka.[8] It can be seen that the dynamics at this step is similar in both structures.

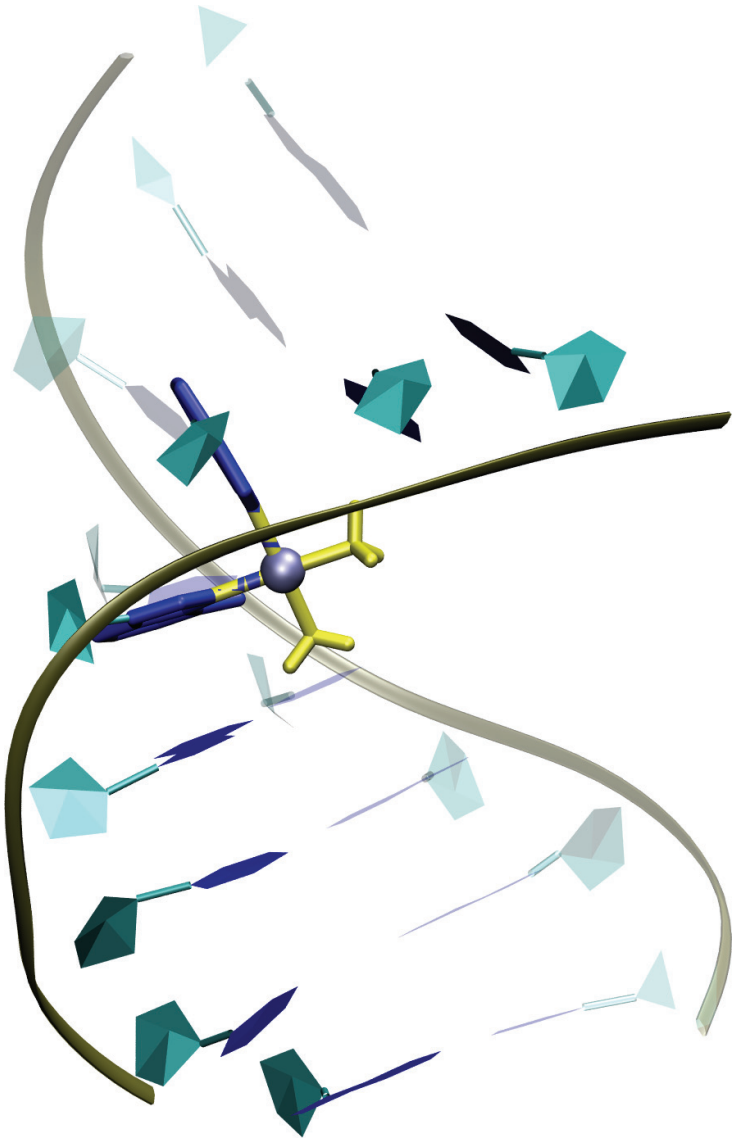

Figure 7. Structure of the G*G*G oligomer averaged over 10 ns and subsequently energy minimised. Guanine bases are represented in blue, platinum in grey and the amines in yellow.

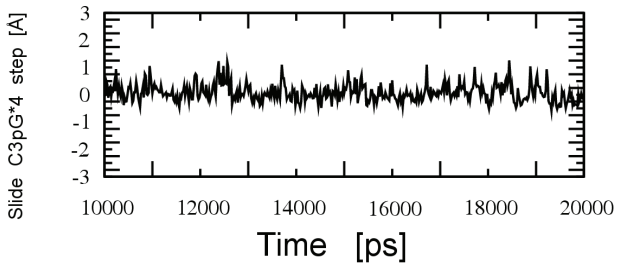

Figure 8. Slide parameter for the C3pG*4 step in G*G*G for the last 10 ns of the MD.

Discussion

The structural perturbation caused by binding of platinum antitumor drugs to DNA has been shown to be specifically recognized by a number of cellular proteins, including HMGB proteins having function in chromatine organization or as transcription factors, repair proteins, or the TATA box binding protein.[38] It is believed that (some of) these recognition proteins mediate the cellular response which finally induces cell death by apoptosis or necrosis.[39] Relatively subtle changes in the adduct structure can affect the recognition and the biological effects in a major way. This is exemplified by the cisplatin analogue oxaliplatin which forms similar GG-Pt adducts to cisplatin. These adducts differ however in repair efficiency, mutagenesis and translesion synthesis. The evaluation of the structural details of the platinum-DNA adducts and of their effects on protein recognition can therefore help to understand why the biological activities of two similar platinum compounds (e.g., cisplatin *versus* oxaliplatin) are different. In this context, Kozelka, Brabec et al. have recently shown that the bases flanking a GG-Pt(diamine) cross-link can affect the structure of the adduct, provided that the diamine has bulky substituents.[40] As far as GG intrastrand adducts of cisplatin are concerned, the Brabec group has shown that the major parameters defining the structural perturbation, namely the kink and unwinding angles, are little affected by the flanking bases[41]. However, in this study, sequences of the type XG*G*G or GG*G*X (X= A, C, T) were not included. For a number of duplex oligonucleotides bearing a G*G*-cisplatin cross-link, detailed structural data based on NMR and/or molecular modelling are available, supporting the idea of basically similar structures.[2, 3] However, these data were limited to pyG*G* sequences and did not include the structural effect of a guanine adjacent to the G*G* cisplatin cross-link. In particular, the influence of a purine flanking the cross-link at the 5′-side is so far unknown.

The results presented here show that the 3′-flanking base has little influence on the G*G* cross-link. From previous studies on G*G*A[7, 8] it was hypothesized that the hydrogen bond between the 3′ flanking A-N7 and the 3′ amino group of cisplatin had a stabilizing effect on the G*G* cross-link and on the BII conformation of the A6pT7 phosphodiester bond. This effect would have been stronger when the 3′ flanking A was replaced by G in G*G*G, but both NMR and MD results failed to show such an effect. In the present case the NMR method may not be sufficiently sensitive to detect the subtle differences between BI and BII conformation.[14] The striking similarity of the chemical shifts in G*G*A and G*G*G, as well as the combined results of all the NMR data and MD simulations, shows that the G*G*A and G*G*G structures are virtually identical.

That both 1,2 and 2,3 G*G* adducts form when a triple-G sequence is platinated is a well-known fact, but the observation of a reversible isomerization on an annealed duplex is unprecedented. The isomerization reaction was followed by 2D NMR and a change from 70:30 to 40:60 (G*G*G:GG*G*) was observed. A characteristic H8-H8 crosspeak between G*5 and G*6 assured that the adduct was indeed an *intra*-strand and not an *inter*-strand cross-link. Although the isomerization reaction was slow, the fact that it resulted in about equal concentrations of the two species makes it reasonable to question the thermodynamic stability of the Pt – G(N7) bond that has generally been regarded as non-labile. This would imply that the models used to describe protein interaction with cisplatin-DNA cross-links should be re-evaluated.

The GG*G* sequence allowed for the first time a 5′-GG* step to be studied. The results show that this step is significantly different from the general class of 5′-pyG* steps and is probably the main reason for the anomalies observed for this structure. Thus, in contrast to the case of the flanking base 3′ to the G*G* cross-link, the presence of a guanine instead of a cytidine or thymine 5′ to the G*G* cross-link seems to have a significant influence on the structure.

Experimental Section

Materials: *cis*-[$PtCl_2{}^{15}NH_3)_2$] was synthesized according to a published method.[42] The oligonucleotides were synthesized and purified (standard purification option) by Eurogentec.

HPLC analysis: HPLC separations were performed with a system consisting of a Waters 626 LC pump, a W600s FlowDetector and a W2487 Dual UV-detector operated by Waters Millennium32 ver. 3.05.01 software on a standard PC. Analytical runs to follow the platination reaction used a POROS R2/10 (100 x 4.6 mm i.d., 10 nm) column (PerSeptive Biosystems GmbH, France) reverse phase column, while the preparative runs used a semipreparative reverse phase column POROS R2/10 (100 x 10 mm i.d., 10 nm) column (PerSeptive Biosystems GmbH, France) . Eluents for both the analytical and preparative runs were: A: ammonium acetate buffer (Merck, 0.5 M, pH 4.5), B: acetonitrile/water (1:1 v/v). An exponential gradient (program 3) from 2% B to 20% B in 25 min was applied, flow rate 5 mL min^{-1} for the analytical column and 10 mL min^{-1} for the semipreparative, performed at room temperature.

Sample preparation: 5 micromoles of the upper strand d(GCCGGGTCGC), quantified by absorbance measurements with the molar extinction coefficient ε assumed to be 88300 $M^{-1}cm^{-1}$ according to Cantor et al.,[35] dissolved in 25 mL of water containing 100 mM $NaClO_4$ and $HClO_4$ to adjust the pH to 4.5, were treated with 1 equiv. of *cis*-[$PtCl_2(^{15}NH3)_2$] at 37 °C at time 0. Another equiv. of *cis*-[$PtCl_2(^{15}NH3)_2$] was added after 20 h, and two additional 0.5 equivs. after 36 and 43 h. The reaction was followed using an analytical HPLC. After 51 h, the reaction was stopped. At this point, two major product peaks eluted at 8.25 and 9.25 min, respectively, while an appreciable amount of the unplatinated oligonucleotide (eluting at 5.3 min) was still present. The two major products were separated using semi-preparative HPLC, lyophilized, desalted using a 1000 MWCO dialysis membrane (Spectrum Labs B.V., The Netherlands) and quantified by UV absorbance measurement (using the same ε as for the unplatinated oligonucleotide). Small samples of each product were radiolabeled and identified using the G-only Maxam-Gilbert sequencing reaction.[43] The major adduct eluting at 8.25 min was identified as the G*4,G*5 platinum chelate and the second adduct eluting at 9.25 min (formed to about half the amount, as judged from the HPLC peak area) as the G*5,G*6 platinum chelate.

The G*4,G*5 platinum chelate was annealed with 1 equiv. of the complementary strand by heating a 500 ul solution with 100 mM $NaClO_4$ and 30 mM phosphate buffer, pH 6.05 at 80 °C for 5 min. The solution was then slowly cooled down to room temperature (within 1 hour) and lyophilized. This double-stranded platinated oligonucleotide was then dissolved in 0.5 mL 99.99% D_2O and re-lyophilized; this procedure was repeated 5 times. Finally, the sample was dissolved in 450 ul of 90:10 H_2O: D_2O (99.96 %) and transferred to a Wilmad 528pp NMR tube for studies of exchangeable protons. The duplex concentration was determined to be 0.30 mM. For the study of non-exchangeable protons the sample was twice lyophilized with 99.6 % and finally re-dissolved in 280 ul 99.96 % D_2O in a Shigemi tube (Sigma-Aldrich). The final solution was 0.50 mM duplex concentration, 55 mM phosphate buffer , 180 mM $NaClO_4$, pH 6.05.

NMR measurements: Spectra were recorded on Bruker Avance DRX 500 and 600 MHz spectrometers at the University of Bergen, Norway and at the Bruker laboratories in Zürich, Switzerland using various multi-resonance gradient probes. While most spectra were recorded at 305K, additional spectra were recorded at various temperatures between 278K and 310K. Several

types of spectra were recorded: 1D ^{1}H and 1D ^{31}P, 2D ^{1}H-^{1}H NOESY, TOCSY, DQF-COSY and E.COSY, 2D ^{1}H-^{31}P HELCO and HETCOSY and 2D ^{1}H-^{15}N HSQC and HMQC. For NOESY spectra, mixing times 80, 150, 200 and 250 ms were used, and mixing times of 50 and 80 ms were used in TOCSY spectra. Presaturation during the recycle delay and the mixing was applied to suppress the H_2O signal for spectra recorded in 90/10 H_2O/D_2O. Further experimental details are given in Supporting Information. ^{1}H shifts were referenced to TSP (Sigma-Aldrich) and ^{31}P shifts to TMP (Sigma-Aldrich). Residual TEAA buffer (ca. 10 mM) from the HPLC purification was detected in the 1-D NMR spectrum. To avoid any loss of sample, we decided not to remove the TEAA buffer.

Distance restraints for use with the MD simulations were calculated from NOESY spectra in D_2O at 305K with mixing times 80, 150 and 200 ms. The ISPA (Isolated Spin Pair Approximation) method was used to derive distances since the low concentration of the sample and the presence of two cisplatin-DNA adducts in solution precluded the use of the full relaxation matrix approach. NOESY cross-peak volumes were referenced to the fixed cytidine H5-H6 distance (2.45 Å). For the NOESY determination of sugar pucker conformation, the accurate measurement of H2′-H6/8 and H3′-H6/8 distances were critical. These distances are especially prone to spin diffusion via the H1′-H2′/H2′′-H6/H8 pathway.[44] Van de Ven & Hilbers examined the correlation between calculated NOESY distances and "true" distances determined from the Arnott B-DNA values.[44] They found a roughly linear correlation, with short distances being overestimated and long distances underestimated by the NOE measurement. Based on their data (Figure 2 of [44]), a linear calibration was applied to the calculated NOESY distances where $r_{calib} = 1.806 \cdot r_{calc} - 1.770$. To account for the uncertainties introduced by the calibration as well as for the relatively low concentration of the samples, an error margin of ±0.6 Å was applied to all distances. Spectra were processed using Topspin (Bruker Biospin, Karlsruhe, Germany) and analysed using Sparky[45].

Melting temperature of d(GCCG*G*GTCGC)-d(GCGACCCGGC): Melting temperature was determined by 1D ^{1}H (512 scans, 32k data points, 22 ppm sweep width) and 1D ^{31}P NMR (128 scans, 32k data points, 12 ppm sweep width). Spectra were recorded at 5K intervals between 278K and 333K in 90/10 H_2O/D_2O and based on line broadening values, the approximate melting temperature was calculated to be 55 °C.

Molecular dynamics simulations and structural analysis: Molecular dynamics (MD) calculations were performed using Amber 6.0[46] and the parm98 force field. The starting structure for **G*G*G** was generated from the all-BI model of **G*G*A**[8] by mutating the A_6T_{15} base-pair into G_6C_{15}, using the program XLEAP from the AMBER suite. This starting model was relaxed by 20 steps of steepest descent energy-minimization followed by a conjugate gradient minimization. This minimized structure was subsequently subjected to a MD simulation using the protocol described by Elizondo-Riojas and Kozelka,[8]. The MD simulation was performed in an orthorombic box of 64*54*54 Å filled with randomly oriented TIP3P water molecules using the PREP, EDIT, LINK, PARM and XLEAP programs of the AMBER suite. The particle-mesh-Ewald (PME) method using charge grid spacing of approx. 1 Å with cubic B-spline interpolation and sum tolerance of 10^{-6} Å was used to calculate the electrostatic energy. A 9 Å cutoff was applied to Lennard-Jones nonbonded terms and for Ewald summations. The temperature was kept at 300 +/-2 K using the Berendsen coupling algorithm. Center of motion was removed every 100 steps of calculation. The SHAKE algorithm was applied to constrain all hydrogen bonds. A snapshot of the simulation was taken each ps. Unrestrained dynamics production was carried out

for 25 ns. The first 5 ns were excluded from analysis since the system was considered not sufficiently equilibrated during that time. The resulting 20000 structures of the MD trajectory were analyzed using the programs CARNAL and PTRAJ from the AMBER suite, CURVES[47], XmGrace (http://plasma-gate.weizmann.ac.il/Grace/), and in-house scripts (http://www.steletch.org), and visualized using the program VMD.[48]

Acknowledgements

We are grateful to Dr. V. Montjardet-Bas for the synthesis of *cis*-[$PtCl_2{}^{15}NH_3)_2$], Dr. S. Bombard for Maxam-Gilbert sequencing, and Dr. H. Kovacs (Bruker Laboratories, Zürich, Switzerland) for recording spectra utilizing a cryoprobe on a Bruker DRX 600 instrument. A stipend for T.S. from the Norwegian Research Council (145183/V30) is gratefully acknowledged. J.K. and S.T. thank the Association for International Cancer Research (AICR) (grant N° 00-321) for financial support. Computer time from the IDRIS computer center of the CNRS and support from COST (Projects D20/003/00 and D20/0006/01), enabling scientific exchange with other research groups, is gratefully acknowledged.

References

[1] V. Murray, H. Motyka, P. R. England, G. Wickham, H. H. Lee, W. A. Denny and W. D. McFadyen, *J. Biol. Chem.* **1992**, *267*, 18805-18809.
[2] S. O. Ano, Z. Kuklenyik and L. G. Marzilli in *Structure and Dynamics of Pt Anticancer Drug Adducts from Nucleotides to Oligonucleotides as Revealed by NMR Methods*, (Ed. B. Lippert), Verlag Helvetica Chimica Acta, Zürich, **1999**, pp. 247-291.
[3] M.-A. Elizondo-Riojas, F. Gonnet, P. Augé-Barrere-Mazouat, F. Allain, J. Bergès, R. Attias, J.-C. Chottard and J. Kozelka in *Molecular Modeling of Platinum Complexes with Oligonucleotides: Methodological Lessons and Structural Insights*, *Vol.* Eds.: L. Banci and P. Comba), Kluwer academic publishers, Dordrecht, **1997**, pp. 131-160.
[4] P. G. Yohannes, G. Zon, P. W. Doetsch and L. G. Marzilli, *J. Am. Chem. Soc.* **1993**, *115*, 5105-5110.
[5] J. M. Villanueva, X. Jia, P. G. Yohannes, P. W. Doetsch and L. G. Marzilli, *Inorg. Chem.* **1999**, *38*, 6069-6080.
[6] V. Monjardet-Bas, J.-C. Chottard and J. Kozelka, *Chem. Eur. J.* **2002**, *8*, 1144-1150.
[7] F. Herman, J. Kozelka, V. Stoven, E. Guittet, J.-P. Girault, T. Huynh-Dinh, J. Igolen, J.-Y. Lallemand and J.-C. Chottard, *Eur. J. Biochem.* **1990**, *194*, 119-133.
[8] M.-A. Elizondo-Riojas and J. Kozelka, *J. Mol. Biol.* **2001**, *314*, 1227-1243.
[9] S. S. Wijmenga, M. M. W. Mooren and C. W. Hilbers in *NMR of nucleic acids; from spectrum to structure*, (Ed. G. C. K. Roberts), Oxford University Press, New. York, **1993**, pp. 218-283.
[10] S. S. Wijmenga and B. N. M. van Buuren, *Prog. Nucl. Mag. Res. Spect.* **1998**, *32*, 287-387.
[11] R. M. Scheek, R. Boelens, N. Russo, J. H. van Boom and R. Kaptein, *Biochemistry* **1984**, *23*, 1371-1376.

[12] D. Yang, S. S. G. E. van Boom, J. Reedijk, J. H. van Boom and A. H.-J. Wang, *Biochemistry* **1995**, *34*, 12912-12920.
[13] A. Gelasco and S. J. Lippard, *Biochemistry* **1998**, *37*, 9230-9239.
[14] S. Teletchéa, B. Hartmann and J. Kozelka, *J. Biomol. Struct. Dyn.* **2004**, *21*, 489-494.
[15] J. H. J. den Hartog, C. Altona, J. H. van Boom, G. A. van der Marel, C. A. G. Haasnoot and J. Reedijk, *J. Biomol. Struct. Dyn.* **1985**, *2*, 1137-1155.
[16] S. U. Dunham, S. U. Dunham, C. J. Turner and S. J. Lippard, *J. Am. Chem. Soc.* **1998**, *120*, 5395-5406.
[17] L. G. Marzilli, J. S. Saad, Z. Kuklenyik, K. A. Keating and Y. Xu, *J. Am. Chem. Soc.* **2001**, *123*, 2764-2770.
[18] F. J. M. van de Ven and C. W. Hilbers, *Nucl. Acids Res.* **1988**, *16*, 5713-5726.
[19] C. Giessner-Prettre and B. Pullman, *Biopolymers* **1976**, *15*, 2277-2286.
[20] L. J. Rinkel and C. Altona, *J. Biomol. Struct. Dyn.* **1987**, *4*, 621-651.
[21] M. R. Conte, C. J. Bauer and A. N. Lane, *J. Biomol. NMR* **1996**, *7*, 190-206.
[22] K. Grzeskowiak, K. Yanagi, G. G. Privé and R. E. Dickerson, *J. Biol. Chem.* **1991**, *266*, 8861-8883.
[23] H.-O. Bertrand, T. Ha-Duong, S. Fermandjian and B. Hartmann, *Nucl. Acids Res.* **1998**, *26*, 1261-1267.
[24] R. J. Isaacs and H. P. Spielmann, *J. Mol. Biol.* **2001**, *311*, 149-160.
[25] K. Wecker, M. C. Bonnet, E. F. Meurs and M. Delepierre, *Nucl. Acids Res.* **2002**, *30*, 4452-4459.
[26] V. A. Roongta, C. R. Jones and D. G. Gorenstein, *Biochemistry* **1990**, *29*, 5245-5258.
[27] J. Falbe and M. Regitz in *Römpp Chemie-Lexikon*, Georg Thieme Verlag, Stuttgart, **1995**.
[28] J. A. Parkinson, Y. Chen, Z. Guo, S. J. Berners-Price, T. Brown and P. J. Sadler, *Chem. Eur. J.* **2000**, *6*, 3636-3644.
[29] Y. B. Wu, P. Pradhan, J. Havener, G. Boysen, J. A. Swenberg, S. L. Campbell and S. G. Chaney, *J. Mol. Biol.* **2004**, *341*, 1251-1269.
[30] A. T. M. Marcelis, C. G. van Kralingen and J. Reedijk, *J. Inorg. Biochem.* **1980**, *13*, 213-222.
[31] A. T. M. Marcelis, C. Erkelens and J. Reedijk, *Inorg. Chim. Acta* **1984**, *91*, 129-135.
[32] J. H. J. den Hartog, C. Altona, J. H. van Boom, A. T. M. Marcelis, L. J. Rinkel, G. Wille-Hazeleger and J. Reedijk, *Eur. J. Biochem.* **1983**, *134*, 485-495.
[33] C. J. Van Garderen, C. Altona and J. Reedijk, *Inorg. Chem.* **1990**, *29*, 1481.
[34] M. Polak, J. Plavec, A. Trifonova, a. Földesi and J. Chattopadhyaya, *J. Chem. Soc. Perkin Trans. I* **1999**, 2835-2843.
[35] Charles R. Cantor, Myron M. Warshaw and H. Shapiro, *Biopolymers* **1970**, *9*, 1059-1077.
[36] T. Cheatham, *J. Biomol. Struct. Dyn.* **1999**, *16*, 845-862.
[37] P. Varnai, D. Djuranovic, R. Lavery and B. Hartmann, *Nucl. Acids Res.* **2002**, *30*, 5398-5406.
[38] D. B. Zamble and S. J. Lippard in *The Response of Cellular Proteins to Cisplatin-Damaged DNA*, (Ed. B. Lippert), Verlag Helvetica Chimica Acta, Zürich, **1999**, pp. 73-110.
[39] J. R. Jamieson and S. J. Lippard, *Chem. Rev.* **1999**, *99*, 2467-2497.
[40] O. Delalande, J. Malina, V. Brabec and J. Kozelka, *Biophys. J.* **2005**, *88*, 1-11.
[41] K. Stehlikova, H. Kostrhunova, J. Kasparkova and V. Brabec, *Nucl. Acids Res.* **2002**, *30*, 2894-2898.
[42] C. Boreham, *Austr. J. Chem.* **1981**, *34*, 659-664.

[43] S. Redon, S. Bombard, M.-A. Elizondo-Riojas and J.-C. Chottard, *Biochemistry* **2001**, *40*, 8463-8470.
[44] F. J. M. van de Ven and C. W. Hilbers, *Eur. J. Biochem.* **1988**, *178*, 1-38.
[45] T. D. Goddard and D. G. Kneller, *Sparky 3*, University of California, San Francisco.
[46] D. A. Case, D. A. Pearlman, J. W. Caldwell, T. E. Cheatham III, W. S. Ross, C. L. Simmerling, T. A. Darden, K. M. Merz, Jr., R. V. Stanton, A. L. Cheng, J. J. Vincent, M. Crowley, V. Tsui, R. J. Radmer, Y. Duan, J. Pitera, I. Massova, G. L. Seibel, U. C. Singh, P. K. Weiner and P. A. Kollman, *AMBER 6*, University of California, San Francisco, **1999**.
[47] R. Lavery and H. Sklenar, *J. Biomol. Struct. Dyn.* **1989**, *6*, 655-667.
[48] A. Dalke, W. Humphrey and J. Ulrich, *VMD (Visual Molecular Dynamics)*, Theoretical Biophysics Group, University of Illinois and Beckman Institute, Urbana, USA, **1997**.

Supplementary information

Cisplatin Adducts on a GGG Sequence Within a DNA Double-stranded Decamer Studied by NMR Spectroscopy and Molecular Dynamics Simulations

Stéphane Teletchéa,[a] Tormod Skauge,[b] Einar Sletten,[b] Jiří Kozelka*[a]

[a] Dr. S. Teletchéa,[+] Dr. J. Kozelka
Laboratoire de Chimie et Biochimie Pharmacologiques et Toxicologiques
Université René Descartes, UMR 8601 CNRS
45, rue des Saints-Pères, 75270 Paris (France)
Fax: +331 42 86 83 87
E-mail: jiri.kozelka@univ-paris5.fr

[b] T. Skauge,[+] Prof. E. Sletten,
Department of Chemistry
University of Bergen
Allégt. 41
5007 Bergen (Norway)

[+] These two authors contributed equally to the present work.

Table of Contents:

NMR experimental details:

Spectra were recorded on Bruker Avance DRX 500 and 600 MHz spectrometers at the University of Bergen, Norway and on a Bruker Avance DRX 600 fitted with a cryoprobe at the Bruker laboratories in Zürich, Switzerland. The experiments in Bergen used a 5 mm multichannel inverse probehead with gradients. Most spectra were recorded at 305 K, additional spectra were recorded at various temperatures between 278 K and 310 K.

For 2D NOESY spectra, mixing times 80, 150, 200 and 250 ms were used. Typically, between 32 and 80 transients were recorded with 2048 experimental points in t_2 for each of 512 or 1024 t_1 increments. Sweep widths of 10 or 22 ppm were used for experiments in D_2O or 90/10 H_2O/D_2O, respectively. For experiments in D_2O, the residual HDO peak was suppressed by a soft presaturation pulse, typically 55-60 dB. Experiments in 90/10 H_2O/D_2O used the dpfgsew5 or Watergate pulse sequences for suppression of the water peak. The spectra were processed using linear prediction in t_1 for a total matrix of 2048x2048 time domain points and a $\pi/2$ shifted squared sine bell shaped apodization function with line broadening of 0.3 Hz, except in the case of low S/N when a lb of 1.0 or 2.0 Hz was used.

Two-dimensional TOCSY spectra were set up with similar parameters as for NOESY, except for the mixing time being either 50 or 80 ms.

The 2D [^{1}H, ^{15}N] HMQC and [^{1}H, ^{15}N] HSQC NMR spectra were recorded in a phase-sensitive mode with the Echo/Antiecho-TPPI quadrature detection scheme. The ^{15}N spins were decoupled during acquisition and pulsed field gradients were employed to select the proper coherence. No extra pulse sequence was required to suppress water in HMQC spectra (pulse sequence of Palmer et al.{Palmer, 1991 #1593}) and HSQC (pulse sequence of Stonehouse et al.{Stonehouse, 1994 #2714}) acquired in H_2O. The HMQC and HSQC NMR spectra were optimized for $^1J_{N,H}$ = 72 Hz. Spectral width in *F1* was 2006 Hz and in *F2* was 4195 Hz, 2048 complex points in each FID in t_2 and 64 increments in t_1, 4-16 transients were averaged for each increment, and a relaxation delay of 2 s was used.

Figure S1. HPLC chromatogram showing the changes in peak intensities as a function of time. Samples were taken from the reaction mixture of single-stranded 5′-d(GCCGGGTCCGC) – 3′ and ^{15}N-labelled cisplatin.

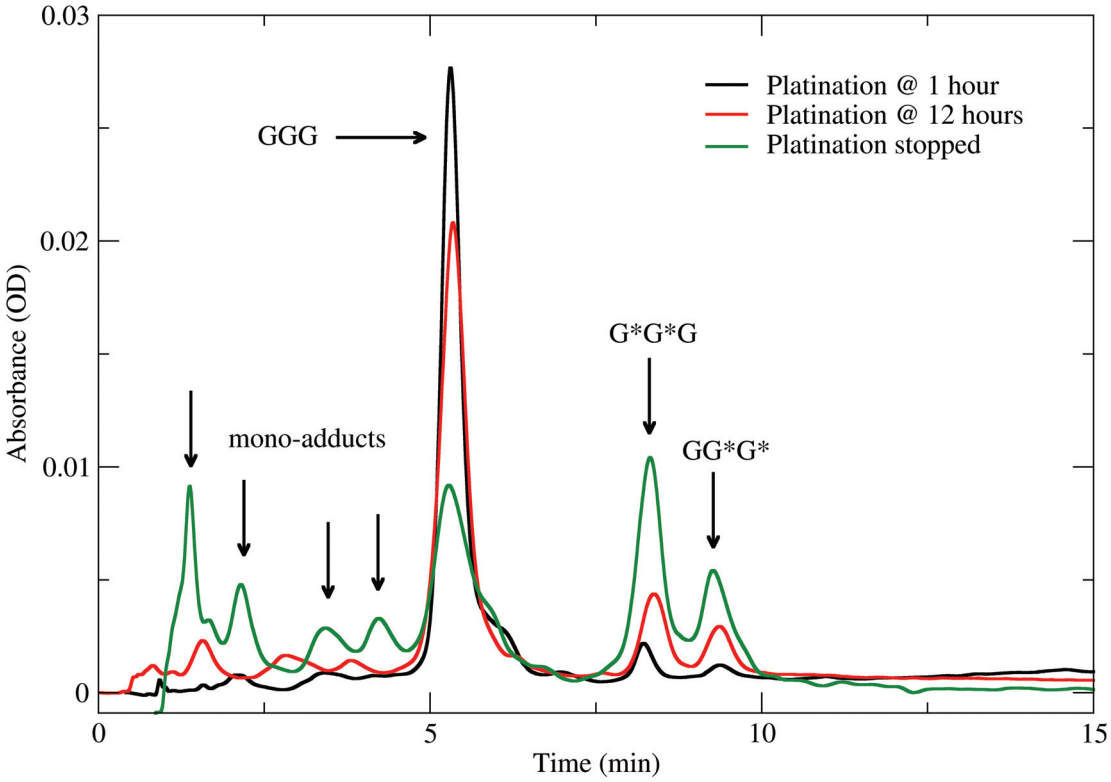

Figure S2. 1D ^{31}P spectrum of the G*G*G/GG*G* mixture.

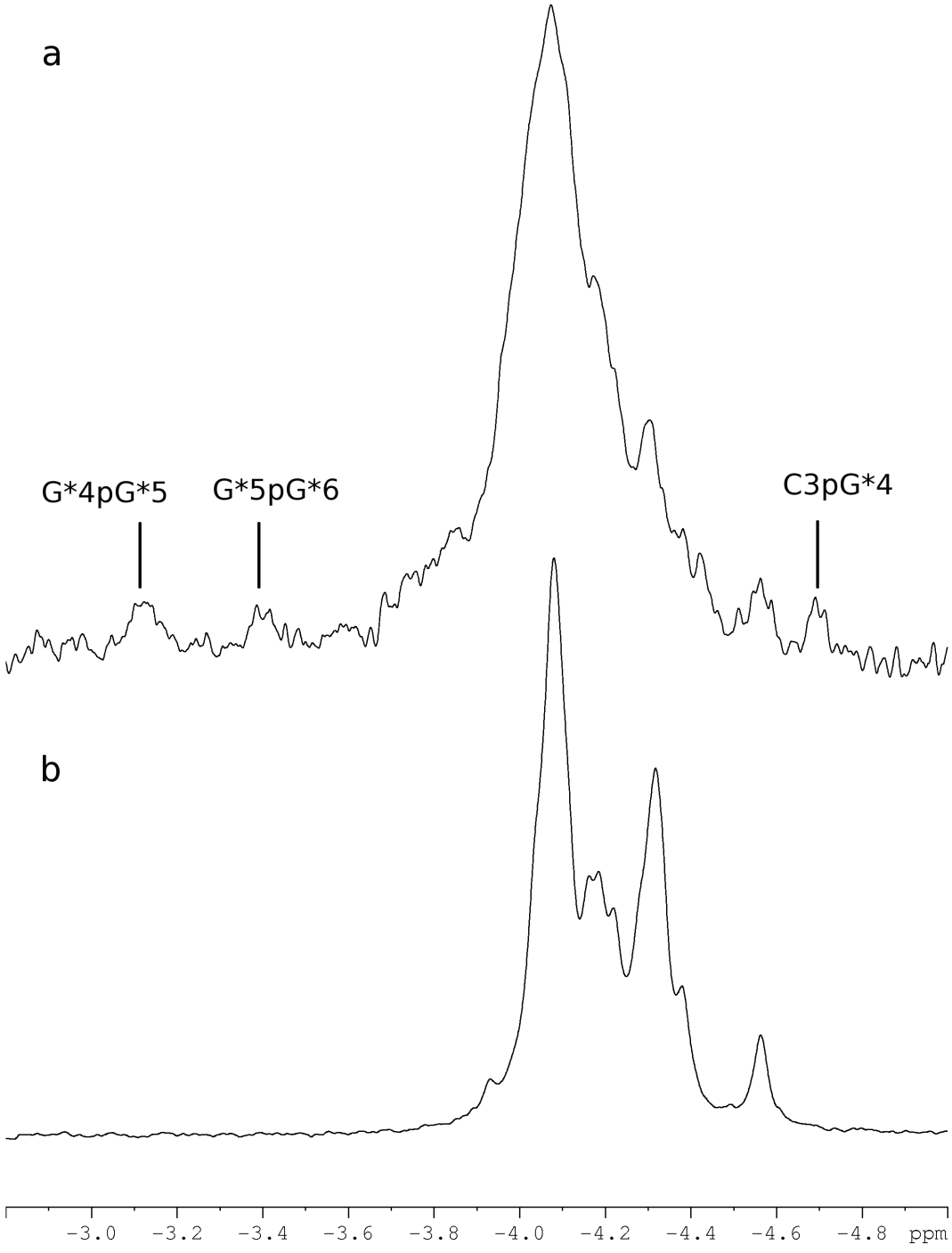

^{31}P NMR spectrum of G*G*G/GG*G* (a) and GGG (b). Spectra recorded at 305K , shift referenced to TMP, concentrations 2 mM and 0.5 mM for GGG and the G*G*G/GG*G* mixture, respectively.

Figure S3. Differential chemical shifts of the non-exchangeable protons of GG*G* minus G*G*A. Spectra recorded at 305K (GG*G*) and 298K (G*G*A). Not all chemical shifts were assigned for GG*G* (see Table 1).

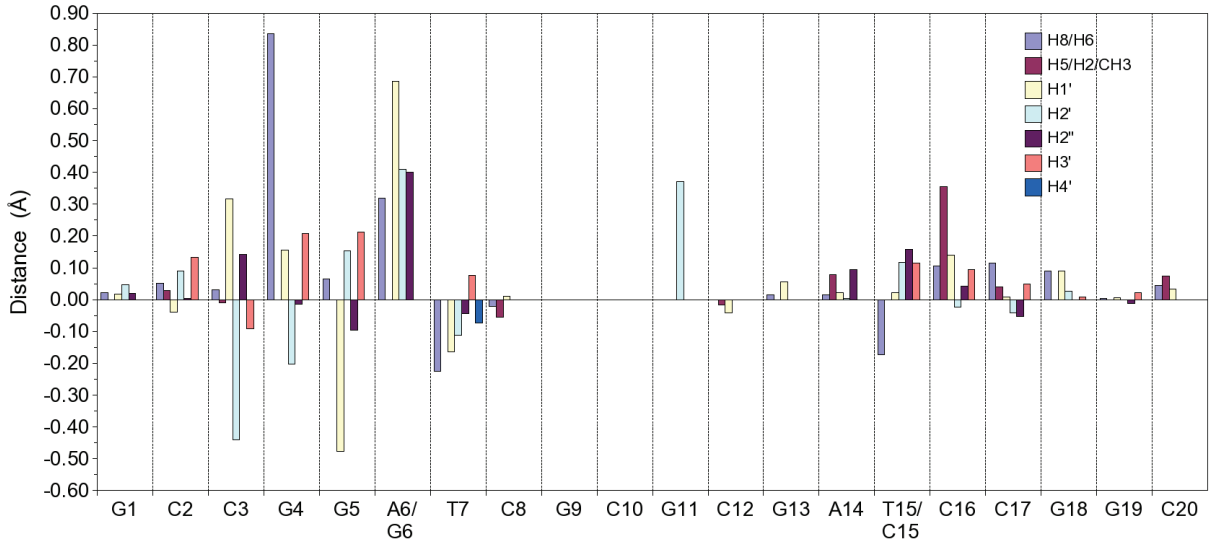

Figure S4. Differential chemical shifts of the non-exchangeable protons of GG*G* minus GGG. Both spectra recorded at 305K. Not all chemical shifts were assigned for GG*G* (see Table 1).

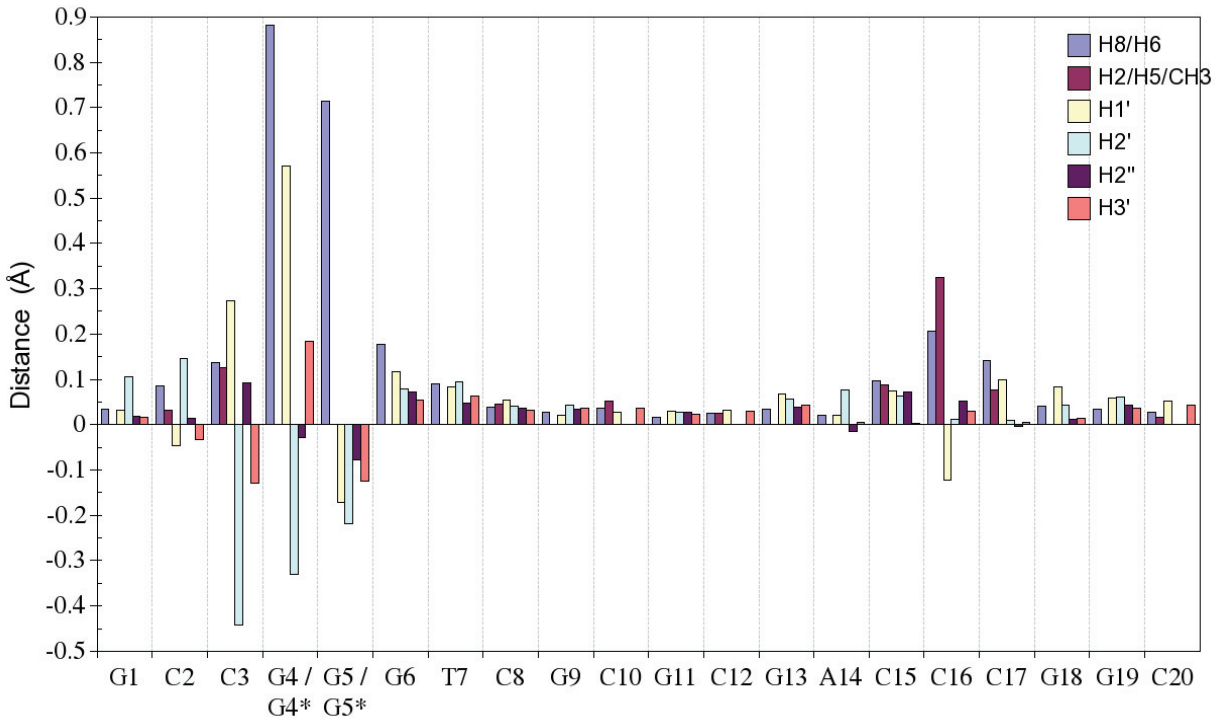

Table S1. Experimental values for the G*G*G:GG*G* ratio as a function of time, derived from Cytidine H5-H6 crosspeak values (see text).

Experiment	Recording Date	Time	Pct Migrated (int)	Pct Major (int)	Ratio (avg)
GGGPt 305K H2O	05/08/03	9	32	68	2.3
GGGPt 305K D2O	17/10/03	82	42	58	1.4
GGGPt 305K D2O tocsy 50ms	08/11/03	104	43	57	1.3
GGGPt 305K D2O	02/02/04	190	55	45	0.8
GGGPt Z 291K H2O 80ms	01/04/05	614	56	44	0.7
GGGPt Z 281K H2O	08/04/05	621	50	50	0.7
GGGPt Z 305K H2O	17/05/05	660	56	44	0.6

Table S2. Comparison sugar pucker conformations derived from NMR and MD results for G*G*G.

	$\%S_{NMR}$[a]	$\%S_{MD}$		$\%S_{NMR}$[a]	$\%S_{MD}$
G1	-/97	100	**G11**	-/94	100
C2	81/90	100	**C12**	98/112	99
C3	36/44	22	**G13**	-/106	99
G4*	12/(-3)	21	**A14**	87/76	90
G5*	89/82	100	**C15**	45/64	66
G6	-/96	100	**C16**	84/57	5
T7	90/89	100	**C17**	96/104	97
C8	86/94	100	**G18**	-/82	100
G9	-/99	99	**G19**	-/90	100
C10	-/86	96	**C20**	-/-	97

[a]Values (A/B) are calculated from A) J-coupling and B) the ratio d(H2′-H6/8):d(H3′-H6/8).

Table S3. NMR and MD derived distances for the interaction site in the context - d(CG*G*G)·(CCCG).

R1 = Residue 1; N1 = Nucleotide 1; R2 = Residue 2; N2 = Nucleotide 2; NMRavg = calculated distance from 2D NOESY volumes; NMRdev = estimated uncertainty (set conservatively due to low concentration and overlapping peaks); MDavg = the distance measured in the MD calculations, averaged over 10 ns; MDdev = deviation of the distance measured over 10 ns; MDmax = the maximum value observed in the simulation; MDmin = the minimum value observed in the simulation; Abs.Diff = the absolute difference between NMRavg and MDavg; >0.60 = disagreement of NMRavg and MDavg larger than 0.60 Å; >0.85 = disagreement of NMRavg and MDavg larger than 0.85 Å (0.85 Å is the uncertainty of the difference if both NMRdev and MDdev are equal to 0.60 Å); >1.00 = disagreement of NMRavg and MDavg larger than 1.00 Å.

R1	N1	Atom1	R2	N2	Atom2	NMRavg	NMRdev	MDavg	MDdev	MDmax	MDmin	Abs.Diff.	>0.60	>0.85	>1.00
3	C	H2´	3	C	H1'	2.71	0.60	2.82	0.10	3.18	2.33	-0.11			
3	C	H2´	3	C	H6	2.80	0.60	3.16	0.32	4.10	1.99	-0.36			
3	C	H2´	3	C	H2´´	1.80	0.60	1.78	0.05	1.98	1.58	0.02			
3	C	H2´	4	G	H8	3.37	0.60	3.12	0.41	5.46	2.06	0.25			
3	C	H2´´	3	C	H1'	2.42	0.60	2.26	0.10	2.64	1.88	0.16			
3	C	H2´´	3	C	H2´	1.85	0.60	1.78	0.05	1.98	1.58	0.07			
3	C	H2´´	4	G	H8	3.61	0.60	4.22	0.60	6.86	2.27	-0.61	+		
3	C	H5	3	C	H6	2.66	0.60	2.45	0.09	2.74	2.13	0.21			
3	C	H1'	3	C	H6	4.06	0.60	3.72	0.09	4.02	3.37	0.34			
3	C	H1'	4	G	H8	5.87	0.60	5.56	0.46	8.18	3.62	0.31			
3	C	H3'	3	C	H6	3.09	0.60	2.46	0.29	4.34	1.84	0.63	+		
3	C	H3'	4	G	H8	5.06	0.60	4.73	0.40	6.67	3.55	0.33			
3	C	H5	2	C	H6	4.53	0.60	3.93	0.44	6.02	2.38	0.60	+		
3	C	H6	4	G	H8	5.97	0.60	5.51	0.40	7.14	4.04	0.46			
4	G	H1'	4	G	H8	4.43	0.60	3.91	0.09	4.22	3.46	0.52			
4	G	H2´	4	G	H1'	2.71	0.60	2.76	0.09	3.15	2.37	-0.05			
4	G	H2´	4	G	H8	3.49	0.60	2.94	0.31	3.99	2.00	0.55			
4	G	H2´	4	G	H2´´	1.84	0.60	1.78	0.05	1.94	1.58	0.06			
4	G	H2´	4	G	H3'	2.63	0.60	2.41	0.11	2.83	1.96	0.23			
4	G	H2´	5	G	H8	3.21	0.60	3.36	0.39	5.00	2.19	-0.15			
4	G	H2´´	4	G	H8	4.68	0.60	4.17	0.17	4.71	2.24	0.51			
4	G	H2´´	4	G	H2´	1.79	0.60	1.78	0.05	1.94	1.58	0.01			
4	G	H2´´	4	G	H1'	2.39	0.60	2.31	0.10	2.70	1.94	0.08			
4	G	H2´´	4	G	H3'	3.64	0.60	3.03	0.06	3.26	2.61	0.61	+		
4	G	H2´´	5	G	H8	4.54	0.60	5.05	0.37	6.49	2.83	-0.51			
4	G	H3'	4	G	H8	2.44	0.60	2.21	0.22	4.73	1.73	0.24			
4	G	H3'	4	G	H1'	4.50	0.60	3.83	0.09	4.18	3.50	0.67	+		
4	G	H3'	5	G	H8	3.98	0.60	3.57	0.31	6.27	2.64	0.41			

4	G	H8	5	G	H8	3.45	0.60	2.89	0.24	3.85	1.99	0.56			
4	G	H1'	5	G	H8	5.26	0.60	5.63	0.29	6.73	4.13	-0.37			
5	**G**	**H1'**	**5**	**G**	**H8**	4.96	0.60	3.90	0.08	4.15	3.60	1.06	+	+	+
5	G	H1'	6	G	H8	3.76	0.60	4.31	0.62	6.74	2.33	-0.55			
5	G	H2´	5	G	H8	2.65	0.60	2.46	0.20	4.13	1.89	0.19			
5	G	H2´	5	G	H3'	2.96	0.60	2.37	0.10	2.72	1.96	0.59			
5	G	H2´	6	G	H8	3.65	0.60	3.96	0.51	5.86	2.13	-0.31			
5	G	H2´´	5	G	H2´	1.79	0.60	1.79	0.05	1.97	1.57	0.00			
5	G	H2´´	5	G	H3'	2.92	0.60	2.73	0.09	3.08	2.38	0.19			
5	G	H2´´	5	G	H8	3.21	0.60	3.74	0.23	4.86	2.84	-0.53			
5	G	H2´´	6	G	H8	3.59	0.60	3.05	0.47	5.12	1.87	0.54			
5	**G**	**H3'**	**5**	**G**	**H8**	3.48	1.00	4.56	0.20	5.19	3.19	-1.08	+	+	+
5	G	H3'	6	G	H8	4.76	0.60	5.39	0.66	7.47	3.28	-0.63	+		
5	G	H2´	5	G	H1'	3.07	0.60	3.04	0.06	3.23	2.81	0.03			
5	G	H2´´	5	G	H1'	3.35	0.60	2.41	0.11	2.81	2.03	0.94	+	+	
6	G	H1'	6	G	H8	4.43	0.60	3.86	0.09	4.19	3.44	0.57			
6	G	H1'	7	T	H6	4.25	0.60	3.60	0.43	5.38	2.14	0.65	+		
6	G	H2´	6	G	H8	2.56	0.60	2.35	0.17	3.37	1.89	0.21			
6	G	H2´	6	G	H3'	2.93	0.60	2.34	0.10	2.70	1.94	0.59			
6	**G**	**H2´**	**7**	**T**	**H6**	2.99	1.00	4.03	0.39	5.88	2.67	-1.04	+	+	+
6	G	H2´´	6	G	H8	3.40	0.60	3.44	0.28	4.55	2.33	-0.04			
6	G	H2´´	7	T	H6	3.09	0.60	2.63	0.37	4.29	1.86	0.46			
6	G	H3'	6	G	H8	4.46	0.60	4.56	0.20	5.25	3.70	-0.10			
6	**G**	**H3'**	**7**	**T**	**H6**	4.15	1.00	5.27	0.38	6.87	4.28	-1.12	+	+	+
6	G	H8	7	T	H6	4.84	0.60	4.57	0.46	6.60	2.94	0.27			
15	C	H1'	15	C	H6	3.89	0.60	3.72	0.09	4.03	3.31	0.17			
15	C	H1'	16	C	H6	4.14	0.60	4.75	0.58	7.58	2.20	-0.61	+		
15	C	H2´	15	C	H6	2.87	0.60	2.84	0.43	4.16	1.89	0.03			
15	C	H2´´	15	C	H1'	2.49	0.60	2.28	0.12	2.77	1.91	0.21			
15	C	H2´´	15	C	H6	3.44	0.60	4.06	0.31	4.76	2.25	-0.62	+		
15	C	H3'	16	C	H6	4.55	0.60	4.38	0.43	6.34	2.77	0.17			
15	C	H5	14	A	H8	4.44	0.60	4.03	0.46	6.35	2.67	0.41			
15	C	H5	15	C	H6	2.65	0.60	2.45	0.09	2.76	2.12	0.20			
15	C	H1'	14	A	H2	5.05	0.60	4.62	0.59	7.05	2.35	0.43			
15	C	H2´	15	C	H1'	3.04	0.60	2.92	0.12	3.20	2.43	0.12			
15	C	H3'	15	C	H6	3.62	0.60	3.12	0.64	4.86	1.91	0.51			
16	C	H1'	17	C	H6	4.50	1.00	5.46	0.48	7.85	3.02	-0.96	+	+	

16	C	H3'	16	C	H6	2.65	0.60	2.38	0.36	4.63	1.75	0.27			
16	C	H5	15	C	H6	4.66	0.60	3.99	0.41	5.63	2.62	0.67	+		
16	C	H5	16	C	H6	2.38	0.60	2.44	0.09	2.76	2.09	-0.06			
16	C	H6	15	C	H6	4.73	0.60	5.05	0.48	7.77	3.33	-0.32			
16	C	H1'	16	C	H6	4.39	0.60	3.74	0.09	4.12	3.40	0.65	+		
16	C	H2´	16	C	H6	3.05	0.60	3.01	0.34	4.12	1.89	0.04			
16	C	H2´	16	C	H1'	2.94	0.60	2.81	0.10	3.19	2.46	0.13			
16	C	H2´´	16	C	H1'	2.54	0.60	2.26	0.11	2.71	1.91	0.28			
16	C	H2´´	16	C	H6	3.14	0.60	4.10	0.19	4.65	2.34	-0.96	+	+	
17	C	H1'	18	G	H8	4.32	0.60	4.73	0.51	7.05	2.98	-0.41			
17	C	H2´	17	C	H2´´	1.54	0.60	1.78	0.05	1.96	1.57	-0.24			
17	C	H2´	17	C	H6	2.60	0.60	2.35	0.26	4.07	1.84	0.25			
17	C	H2´	18	G	H8	3.83	0.60	3.29	0.50	6.14	1.95	0.54			
17	C	H2´´	17	C	H6	3.77	0.60	3.76	0.22	4.76	2.52	0.01			
17	C	H2´´	18	G	H8	3.71	0.60	3.10	0.51	6.68	1.93	0.61	+		
17	C	H2´´	18	G	H1'	3.75	0.60	4.60	0.30	6.26	3.83	-0.85	+	+	
17	C	H3'	18	G	H8	4.52	0.60	5.06	0.52	7.21	2.99	-0.54			
17	C	H5	16	C	H6	4.23	0.60	3.38	0.37	5.24	2.10	0.85	+		
17	C	H5	17	C	H6	2.48	0.60	2.45	0.09	2.76	2.11	0.04			
17	C	H2´	17	C	H1'	3.74	0.60	3.02	0.07	3.25	2.56	0.72	+		
17	C	H2´´	17	C	H1'	3.07	0.60	2.34	0.11	2.77	1.88	0.73	+		
18	G	H1'	18	G	H8	4.16	0.60	3.77	0.11	4.14	3.17	0.39			
18	G	H1'	19	G	H8	3.72	0.60	2.83	0.30	4.93	1.89	0.89	+	+	
18	G	H2´	18	G	H8	2.63	0.60	2.38	0.16	3.29	1.87	0.25			
18	G	H2´	18	G	H3'	1.97	0.60	2.39	0.10	2.78	2.03	-0.42			
18	G	H2´	19	G	H8	4.94	1.00	4.79	0.33	5.94	3.22	0.15			
18	G	H2´´	18	G	H8	3.18	0.60	3.08	0.26	4.11	2.23	0.10			
18	G	H2´´	19	G	H8	3.63	0.60	3.28	0.43	4.68	1.99	0.35			
18	G	H3'	18	G	H1'	4.07	0.60	3.66	0.09	4.05	3.33	0.41			
18	G	H3'	18	G	H8	3.73	0.60	4.72	0.17	5.38	3.95	-0.99	+	+	
18	G	H8	17	C	H6	4.93	0.60	4.48	0.47	6.82	3.13	0.45			
											SUM		**25**	**10**	**4**